Han, Y., Horsfield, B., Mahlstedt, N., Wirth, R., Curry, D. J., LaReau, H. (2019): Factors controlling source and reservoir characteristics in the Niobrara shaleoil system, Denver Basin. - *AAPG Bulletin*, *103*, 9, pp. 2045—2072.

DOI: http://doi.org/10.1306/0121191619717287

Q:1 *Factors controlling source and reservoir characteristics in the Niobrara shale oil system,* Q:2 *Denver Basin*

Yuanjia Han, Brian Horsfield, Nicolaj Mahlstedt, Richard Wirth, David J. Curry, and Heather LaReau

ABSTRACT

This paper clarifies the controls of oil retention in the Niobrara Formation, Denver Basin, in the western United States. Sweet spots have been recognized using a total of 98 core samples from 5 wells with maturities covering the oil window.

Oil retention in the source rock samples (carbonate content <70 wt. %) is controlled by organic matter richness and thermal Q:6 maturity. In general, the vaporizable hydrocarbon (HC) yield at nominal temperatures at 300°C (572°F) (Rock-Eval S_1) is positively correlated to total organic carbon (*TOC*). With increasing maturity, the so-called oil saturation index ($S_1/TOC \times 100$) first increases until a maximum retention capacity (100 mg HC/g *TOC*) is exceeded at the temperature at the maximum rate of petroleum generation by Rock-Eval pyrolysis (T_{max}) of approximately 445°C (~833°F) and subsequently decreases. The depletion in oil retention capacity is believed to be associated with the appearance of organic nanopores.

Oil retention in samples with distinct reservoir potential (carbonate >30 wt. %) is controlled by carbonate content, which Q:7 is positively related to the amount of retained oil (S_1). Petrographic features indicate that oil or bitumen is stored in porous calcite fossils (i.e., coccolith and foraminifera), which provide additional space for petroleum storage. Chalk samples (carbonate >85 wt. %) are characterized by anomalously low T_{max} values caused by the influence of heavy petroleum or bitumen. The amount of this bitumen is higher than the initial petroleum potential of kerogen in A and B chalks and thus must have been emplaced here. The most likely sources are juxtaposed organic-rich marl layers.

Manuscript received July 12, 2017; provisional acceptance November 14, 2017; revised manuscript received January 9, 2018; revised manuscript provisional acceptance February 6, 2018; 2nd revised manuscript received February 8, 2018; final acceptance January 21, 2019.
DOI:10.1306/0121191619717287

AUTHORS

YUANJIA HAN ~ *German Research Centre for Geosciences (GFZ), Telegrafenberg, Potsdam, Germany; Key Laboratory of Tectonics and Petroleum Resources, China University of Geosciences, Wuhan, China; yuanjia@gfz-potsdam.de; hanyj@cug.edu.cn*

Yuanjia Han is a junior professor at China University of Geosciences, focusing primarily on hydrocarbon retention and migration processes in unconventional shale systems. He obtained his B.S. and M.S. degrees from China University of Geosciences and a Ph.D. from the Technical University of Berlin, both with specialization in integrated petroleum systems analysis. He is the corresponding author.

BRIAN HORSFIELD ~ *Section on Organic Geochemistry, GFZ, Telegrafenberg, Potsdam, Germany; horsf@gfz-potsdam.de*

Brian Horsfield was a full professor of organic geochemistry and hydrocarbon systems at the Technical University of Berlin, Germany, as well as leader of organic geochemistry at the GFZ. He is a member of the German Academy of Science and Technology. He has more than 30 years of experience working with and for industry in upstream research and development. The evaluation of gas in place and producibility in unconventional hydrocarbon systems of the United States, South Africa, China, Australia, and North Africa are key activities in his service and research at the present time.

NICOLAJ MAHLSTEDT ~ *Section on Organic Geochemistry, GFZ, Telegrafenberg, Potsdam, Germany; nicolaj.mahlstedt@gfz-potsdam.de*

Nicolaj Mahlstedt is a postdoctoral researcher at the GFZ. He studied applied geosciences and holds a diploma and Ph.D. from the Technical University of Berlin. He conducted his Ph.D. within the GFZ–Industry Partnership Program investigating high temperature methane generation. His major scientific interests include petroleum system analysis, oil and gas retention processes, compositional kinetic modeling, and the development of geochemical screening tools.

Q:3

RICHARD WIRTH ~ *Section on Chemistry and Physics of Earth Materials, GFZ, Telegrafenberg, Potsdam, Germany; wirth@gfz-potsdam.de*

Richard Wirth is a senior research scientist and laboratory supervisor at the GFZ. He studied mineralogy and electron microscopy and holds a diploma and Ph.D. from the University of Würzburg. His work is focused on the application of advanced electron microscopy (transmission electron microscopy and focused ion beam).

DAVID J. CURRY ~ *Noble Energy, Inc., Houston, Texas; David.Curry@nblenergy.com*

David J. Curry is a senior geochemical advisor with the Geoscience Technology Organization at Noble Energy. He received his Ph.D. from The University of Texas at Austin in 1981 with a specialty in organic geochemistry. Since then, he has worked in petroleum systems analysis (basin modeling and geochemistry) in both research and exploration positions at several petroleum companies, including ExxonMobil, Conoco, Devon, HRT Petroleo, and Noble. His interests include nonmarine petroleum systems; source-facies depositional processes; kinetics and generation, expulsion, and migration processes and their effects on yields and fluid properties; and the characterization of geopolymers.

HEATHER LAREAU ~ *Noble Energy, Inc., Denver, Colorado; heatherthegeologist@gmail.com; Heather.Lareau@bp.com*

Heather L. LaReau is currently the geoscience manager for the West Business Unit within BP's Lower 48. She received her M.Sc. degree from McMaster University in 2001 with a concentration in geoarchaeology, stratigraphy, and radiometric dating methods. In 2007, she received her Ph.D. from the University of Wyoming with a focus on fluvial sedimentology and stratigraphy (characterizing avulsion processes in the rock record) throughout Rocky Mountain basins. Her industry career has been based in Denver, Colorado, working unconventional oil and gas assets, exploration, reservoir characterization, and geochemistry at EnCana, Noble Energy, and, most recently, BP's Lower 48. Her

Thus, sweet spots occur where carbonate content is either low (high *TOC*) or high (low *TOC*), whereas production of petroleum from the pore space of presumably brittle chalk seems more attractive than production from organic- and clay-rich rocks.

INTRODUCTION

Shale oil systems are organic-rich mudstone units in which a significant portion of the generated oil is retained in situ or has migrated into juxtaposed organic-lean rocks (e.g., carbonates) (Jarvie, 2012). The Upper Cretaceous Niobrara Formation fits this description perfectly, with a combination of interbedded organic-rich mudstones and relative organic-lean chalks.

The Niobrara strata were deposited in the Western Interior Seaway (WIS) during the late Turonian to early Campanian (89–82 Ma) (Da Gama et al., 2014). During that time (Figure 1A), the WIS stretched from the Arctic Ocean in the north, extending through Canada and the United States, all the way to the Gulf of Mexico in the south (Kauffman, 1977). Rhythmic stratification of chalk-marl beds is characteristic of the Niobrara Formation (Locklair and Sageman, 2008). Brought about by the variation of siliciclastic input, the rhythmical bedding is believed to have been controlled by eustatic and climatic cycles (Pollastro, 2010). In the Denver Basin, periods of prevailing cold currents from the Arctic Ocean in the north resulted in the deposition of marls (Luneau et al., 2011; Da Gama et al., 2014) in which terrestrial detritus was primarily sourced from the western uplifts (Figure 1A). Thus, the Niobrara strata become progressively siliciclastic to the north, west, and northwest (Pollastro, 2010).

Stratigraphically, the Niobrara Formation overlies the Carlile Shale and is overlain by the Sharon Springs Member of the Pierre Shale (Figure 1B). The lower limestone part is known as the Fort Hays Member, and the upper units, namely "A," B," and "C" chalk and marl intervals, are grouped together as the Smoky Hill Member. The chalks and marls are considered as the major hydrocarbon (HC) reservoirs (Sonnenberg and Weimer, 1993; Jarvie, 2012; Welker et al., 2013) and source rocks (Landon et al., 2001), respectively. The marls, formed under suboxic-to-anoxic bottom water conditions (Tanck, 1997; Da Gama et al., 2014), are characterized by relatively high contents of type II organic matter (OM) (Luneau et al., 2011; Sonnenberg, 2011). Thermal maturity of the kerogen ranges from immature (thermal stress equivalent <0.6% vitrinite reflectance [R_o]) in the eastern flank of the Denver Basin to gas-condensate mature (1.4% R_o) in the western Wattenberg gas field (Higley et al., 2003; O'Neal, 2015).

Petroleum exploration activities in the Denver Basin date back to 1881 when the first oil well was drilled in the Florence field (Figure 1A), which is the oldest continuously working oil field in the United States (Higley, 2015). More than 1.3 billion bbl of oil and 7.4 trillion ft^3 of gas have been produced from the basin's more than 47,000 conventionally drilled vertical wells. Thermogenic gas accumulations are concentrated along the axis of the Denver Basin in the Wattenberg gas field (Sherwood et al., 2013) where the deeply buried source rocks have entered the gas window (Higley et al., 2003). Going eastward, the gently dipping basin flank is buried to only shallow depth. Biogenic gas is produced from the immature Niobrara Formation in the eastern basin that extends farther eastward into Kansas and Nebraska (Rice, 1984) (Figure 1A). Petroleum has been produced from various strata with depths ranging from less than 900 ft (<270 m) of the Pierre Shale in the Florence field to approximately 10,000 ft (~3000 m) of the Muddy (J) Sandstone in the Wattenberg gas field (Higley, 2015). The Niobrara Formation has been an active HC play in the Denver Basin since the mid-1970s (Pollastro, 2010), and the production was substantially accelerated in the early 1990s because of the onset of horizontal drilling as exemplified in the Silo field (Welker et al., 2013). The Silo field is located in the northern part of the basin in Wyoming (Figure 1A). Oil-bearing natural fractures are concentrated there in the more brittle chalk units and are recognized as being important for storage and production of HCs (Sonnenberg and Weimer, 1993; Welker et al., 2013). Although oil production in the Silo field decreased sharply throughout the early 2000s, the application of multistage hydraulic fracturing brought about a renaissance in exploration activity throughout the whole Rocky Mountain region (Siguaw and Estes-Jackson, 2011a, b). In the Denver Basin, significant amounts of unconventional oil have been produced from the oil-mature and brittle chalk units, especially from the B-chalk interval (Jarvie, 2012). As of 2017, liquid production from the newly drilled Niobrara wells has reached 1300 bbl/day per rig, and natural gas production was steady at approximately 4400 ft^3/day per rig (US Energy Information Administration, 2017).

The current study aims at clarifying the controls for oil retention in the Niobrara shale oil system in the Denver Basin so that zones of enrichment can be recognized. In general, the retention of petroleum in organic-rich shales is controlled mainly by the sorption capacity of its OM (Baker, 1962; Tissot et al., 1971; Stainforth and Reinders, 1990; Pepper, 1991), and a retention threshold of 100 mg HC/g total organic carbon (TOC) has been proposed (Sandvik et al., 1992; Jarvie, 2012), irrespective of OM type and thermal maturity. Interestingly, Han et al. (2015) reported that the shale intervals most enriched in petroleum are not necessarily associated with the OM richest layers but with associated porous biogenic matrices. Another key

interests include depositional processes; petroleum system characterization; generation, expulsion, and migration processes; innovation; and unconventional resource plays and exploration.

ACKNOWLEDGMENTS

We wish to thank Andrew Pepper, Tongwei Zhang, and Norelis Rodriguez for their careful reviews and useful comments. The editorial comments and suggestions by AAPG Editor Barry J. Katz and Stephen C. Ruppel are also gratefully acknowledged. This work was carried out in the framework of Yuanjia Han's at the Technical University of Berlin, which was sponsored by the China Scholarship Council and Noble Energy. We express our gratitude to Anja Schleicher, Elke Lewerenz, Ilona Schäpan, and Anja Schreiber for their technical support in GFZ. Special thanks are due to Marshall Deacon and Richard George for their helpful collaborations in Noble Energy.

DATASHARE XX

Tables S1–S5 are available in an electronic version on the AAPG website (www.aapg.org/datashare) as Datashare XX.

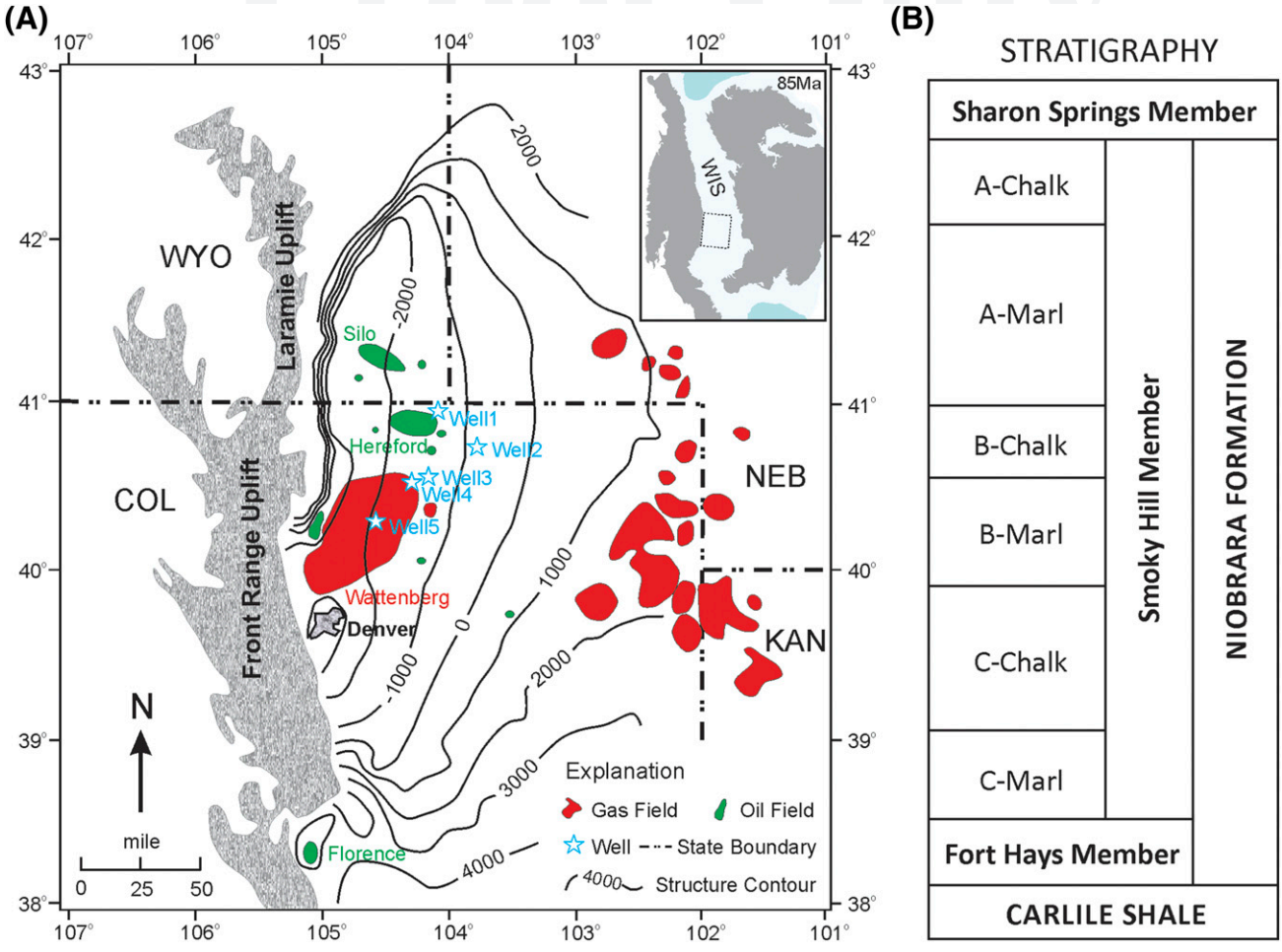

Figure 1. (A) Structural map of the Denver Basin showing the locations of the study wells. Detailed information concerning name and location of wells is confidential. The development of Western Interior Seaway (WIS) during the Late Cretaceous (85 Ma) is shown in the inset figure in which the study area is marked by a rectangle. Contours of top Niobrara Formation are in feet relative to sea level. Modified from Sonnenberg (2011). (B) Generalized stratigraphic column of the Denver Basin showing the Upper Cretaceous Niobrara Formation (89–82 Ma). Modified from Pollastro (2010). COL = Colorado; KAN = Kansas; NEB = Nebraska; WYO = Wyoming.

topic concerning the exploration of shale plays is predicting the occurrence of organic pores. Organic pore development is commonly stated to be largely caused by the thermal cracking of kerogen and bitumen, following the pioneering work of Loucks et al. (2009) and Bernard et al. (2012b), respectively. Numerous studies have actually revealed that organic pores can develop over a wide range of maturities (Loucks et al., 2009; Curtis et al., 2011, 2012; Bernard et al., 2012a, b; Brian et al., 2013; Jennings and Antia, 2013; Milliken et al., 2013; Loucks and Reed, 2014; Pommer and Milliken, 2015; Reed and Loucks, 2015; Ko et al., 2016, 2017; Mathia et al., 2016; Han et al., 2017), but it is still unclear how exactly organic pores are developed in the Niobrara shale oil play and whether they play a role in the retention or storage of oil. The current study uses a multifaceted approach, including x-ray diffraction (XRD), optical microscopy, scanning electron microscopy (SEM), transmission electron microscopy (TEM), Rock-Eval, and open-system pyrolysis gas chromatography (Py-GC) to address these issues.

METHODOLOGY

X-Ray Diffraction

A total of 98 core samples selected from 5 wells (Tables S1–S5, supplementary material available as AAPG Datashare XX at www.aapg.org/datashare)

along a north-to-south profile (Figure 1A) were prepared for x-ray powder diffraction measurements. Core samples were roughly pulverized and extracted for 48 hr at 60°C (140°F) in a Soxhlet apparatus (Soxhlet, 1879) using a ternary azeotropic solvent system (30:38:32 for methanol, acetone, chloroform, respectively). Extracted samples were then milled in a McCrone Micronizing Mill in cyclohexane for 10 min to assure uniform grain sizes (<10 μm [0.39 mil]). Diffraction data were recorded from 5° to 85° 2θ with a step width of 0.013° and a scan time of 60 s per step. We collected x-ray patterns using a Malvern Panalytical Empyrean powder diffractometer with Cu–K-α radiation, automatic divergent, and antiscatter slits and a PIXcel^{3D} detector. Qualitative mineral phase identification was achieved by automatic search-and-match procedures of the DIFFRAC^{plus} software EVA (Bruker AXS). Semiquantitative mineral analysis was carried out using the Rietveld algorithm BGMN (Bergmann et al., 1998) by the software AutoQuant (General Electric Sensing and Inspection Technologies).

Thin Section: Scanning Electron Microscopy

An optical microscope and a scanning electron microscope were used to complement mineral characterization. Thin sections were mechanically polished and analyzed under transmitted white light, reflected white light, and blue excitation fluorescent light to reveal organic–inorganic relationships. We conducted SEM conducted on Au- and Pd-coated thin sections and rock fragments. Backscattered electron and secondary electron images were taken with a 12.5-mm (0.49-in.) working distance. We performed x-ray stage mapping for Si, Mg, Ca, Al, Fe, S, and C by energy-dispersive spectroscopy using a 20-kV accelerating voltage.

Focused Ion Beam–Transmission Electron Microscopy

To evaluate the roles played by organic pores on the retention of oil within organic-rich shales, TEM foils with dimensions of 15–20 μm × 10 μm × 0.15 μm (0.59-0.79 mil × 0.39 mil × 0.0059 mil) were prepared using focused ion beam (FIB) following the procedure described in previous reports (Wirth, 2004, 2009). Rock chips were first mechanically polished and coated with a conducting material (e.g., Au) before FIB milling. During foil milling, the gallium ions were accelerated in an electrical field up to 30 kV for sputtering atoms from the target material. We performed TEM with a Tecnai F20 X-Twin transmission electron microscope with a field emission gun electron source. The TEM was operated at 200 kV, with a nominal camera length of 330 mm (13 in.). We acquired TEM images as high-angle annular dark-field images in Z-contrast mode or as energy-filtered images applying a 200-kV window to the zero-loss peak. Energy-dispersive x-ray spectroscopy (EDXS) scanning was carried out using an EDXS x-ray analyzer with an ultrathin window. We performed EDXS particularly within organic particles to determine possible structural changes induced by high-energy electrons (e.g., 200 kV).

Rock-Eval Pyrolysis and Total Organic Carbon Content Determination

To evaluate the effects of retained oil on Rock-Eval data and to assess total oil in place following ideas reported in Han et al. (2015), Rock-Eval pyrolysis (Espitalié et al., 1977) was performed on both pulverized whole rocks and solvent-extracted samples (98 in total) using a Rock-Eval 2 instrument. For *TOC* analysis, the finely crushed rock samples were firstly treated with dilute hydrochloric acid (HCl to water at a 1:9 ratio) at 60°C ± 5°C (140°F ± 41°F) to remove carbonate. The percent of carbonate was measured according to the sample weight difference before and after HCl treatment. Afterward, the samples were combusted in oxygen at 1350°C (2462°F) in a Leco SC632 combustion oven. The *TOC* was calculated from the peak area of generated CO_2 recorded by an infrared detector.

Open-System Pyrolysis Gas Chromatography

Open-system Py-GC was carried out on 20 unextracted samples from the least mature well 1 to characterize the labile macromolecular OM on a

molecular level. Milligram amounts of material were placed into a glass tube and purged in a helium flow at 300°C (572°F) for 5 min. Then, the temperature was raised from 300°C to 600°C (572°F to 1112°F) at 50°C/min (122°F/min) and held for 2 min. Generated products were transported and collected in a liquid nitrogen cooled trap (–178°C [–352°F]). After 10 min, products were liberated at 300°C (572°F) and transferred with helium with a flow rate of 30 ml/min into an Agilent gas chromatograph (Gas Chromatograph 6890A series). The temperature of the GC oven was programmed from 30°C to 320°C (86°F to 608°F) at 5°C/min (41°F/min) to mobilize products, which were then measured by flame ionization detector. Product quantification was based on external standardization using n-butane. Prominent peaks were identified by reference chromatograms and using Gas Chromatography ChemStation© software from Agilent Technologies. The protocols of Horsfield et al. (1989) were used for data evaluation.

LITHOLOGY AND SAMPLE CLASSIFICATION

As an analog of the Eagle Ford Shale (Fairbanks et al., 2016; Frébourg et al., 2016), the Niobrara Formation is interpreted to be a binary sedimentary system composed of alternating deposition of carbonates and siliciclastic influx (Locklair and Sageman, 2008). Chalks were reported to have been formed from the accumulation of coccolith-rich oozes (Hattin, 1981), and marl deposition is believed to be driven from variations in siliciclastic input (Locklair and Sageman, 2008). In line with that, the content of carbonate is inversely proportional to the illite–smectite content (Figure 2A) as well as the quartz content (Figure 2B). Both clay minerals (Figure 3J) and quartz (Figure 3C, G, H) show features typical of clastic particles. This points to a common detrital origin corroborated by a positive correlation of contents of quartz and illite–smectite mixed layers (Figure 2C). According to the results of XRD (Tables S1–S5, supplementary material available as AAPG Datashare XX at www.aapg.org/datashare) as well

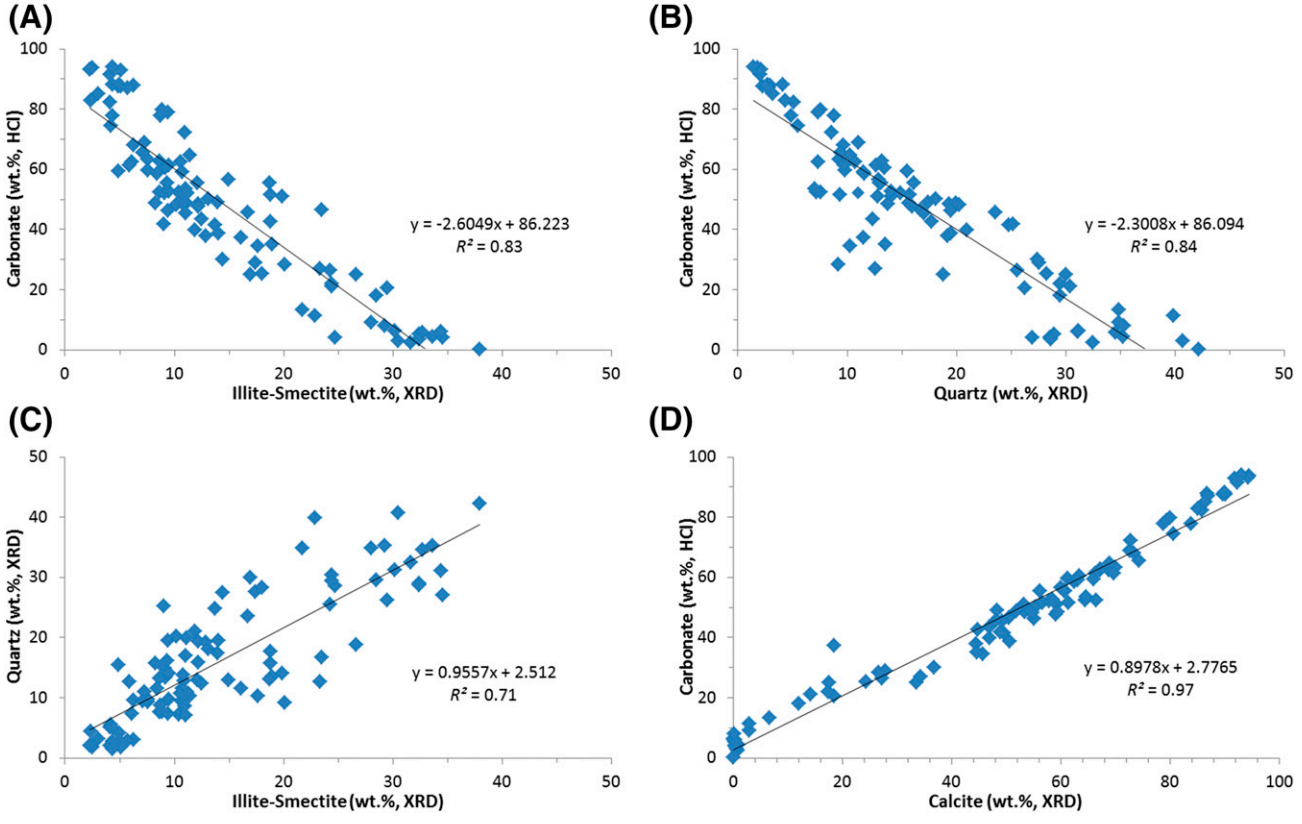

Figure 2. Plots of the content of various minerals. (A) Illite–smectite mixed layers versus carbonate content. (B) Quartz versus carbonate content. (C) Illite–smectite mixed layers versus quartz content. (D) Calcite versus carbonate content. The carbonate content was determined by HCl solution, and the contents of illite–smectite, quartz, and calcite were measured by x-ray diffraction (XRD). R^2 = xxx.

as optical and electron microscopy (Figure 3), calcite is the principal carbonate mineral (Figure 2D). Dolomite can be identified locally (Figure 3G). Low-magnesium calcite consists largely of a micritic matrix (Figure 3A), fecal pellets (Figure 3A), and foraminifera tests (Figure 3B, C). Fecal pellets are enriched in coccolith fragments, without noticeable diagenetic features (Figure 3K, L). Coccolithophores disseminated in the matrix were also commonly observed (Figure 3G, H). Foraminiferal tests are generally cemented by sparry calcite (Figure 3B–D) or less commonly by pyrite framboids (Figure 3G). As an end member of carbonate-siliciclastic sediments, chalk is almost exclusively composed of calcareous fossils (Figure 3K, L) deposited in the form of coccolith-rich oozes.

Chalk units are reported to be the main production reservoirs in the Niobrara play (Sonnenberg and Weimer, 1993; Jarvie, 2012; Welker et al., 2013). The concept of "oil crossover," a phenomenon corresponding to oil saturation index ($OSI = [S_1/TOC] \times 100$) values exceeding 100 mg HC/g *TOC* (Jarvie, 2012), is here used to identify zones containing producible oil. In our Niobrara sample set, a significant increase in *OSI* can be observed for samples with carbonate contents greater than 70 wt. % (Figure 4A). Thus, samples with carbonate greater than 70 wt. % seem to be promising reservoir rocks.

In line with published studies (Ricken, 1996; Tanck, 1997; Landon et al., 2001), carbonate content is negatively correlated with *TOC* content for single wells (well 3; Figure 4B). Samples with carbonate content less than 70 wt. % show *TOC* values exceeding 2.5 wt. % (Figure 4B). Together with the previous identification of promising reservoir rocks (carbonate >70 wt. %), 2.5 wt. % *TOC* can be treated as an empirical criterion for "organic-rich" rocks. In fact, TOC is positively correlated to contents of illite–smectite (Figure 4C) and quartz (Figure 4D). It can be concluded that the richer a sample is in siliciclastic detritus, the higher is its potential of being a source rock. As an end member of carbonate-siliciclastic rocks, Niobrara mudstones are the most potential source rocks.

In general, core samples are named after the intervals from which they were taken from. But in the extremely heterogeneous Niobrara Formation, decimeter-scale rhythmic stratification of chalk-marl beds is characteristic of all intervals. Relating samples to named intervals is useful although not always sufficient. In this case, samples are grouped in terms of mineral composition as well. According to the major lithologies of the Niobrara sample set (Tables S1–S5, supplementary material available as AAPG Datashare XX at www.aapg.org/datashare), chalk is defined as a rock composed of more than 85 wt. % of carbonate (Table 1). Marly chalk is a transition rock type between chalk and marl in which the latter has carbonate contents ranging from 70 to 30 wt. %. Likewise, marly mudstone is treated here as a transition rock type between marl and mudstone, whereas the latter mainly consists of fine siliciclastic debris (quartz, feldspar, clay, mica, etc.) with carbonate content less than 15 wt. % (Table 1).

Overall, the chalks and marly chalks are relatively organic-poor rocks (*TOC* <2.5 wt. %) showing reservoir potential, whereas the organic-rich (*TOC* >2.5 wt. %) marl-mudstones are potential source rocks (Table 1). This classification fits previous reports indicating that marls are the major source rocks (Landon et al., 2001; Luneau et al., 2011). However, the 2.5 wt. % TOC cutoff value is just an empirical criterion, and it should not be forgotten that kerogen type and maturity are also critical parameters in determining an effective source rock (Tissot and Welte, 1984).

SOURCE ROCK CHARACTERISTICS

Type and Maturity of Source Rocks

Hydrogen index (*HI*) and oxygen index (*OI*) values of unextracted source rock samples exhibiting carbonate contents <70 wt. % are shown in a pseudo Van Krevelen diagram for kerogen typing (Figure 5). Confirming earlier results of Landon et al. (2001) and Sonnenberg (2011), the majority of Niobrara samples plot on the evolution pathway for type II kerogens (Figure 5). Exceptions are samples from the Fort Hays Member that seem to be of lower quality falling on the kerogen type III trend line. The overlying Sharon Springs Member also appears to contain type II kerogen, whereas kerogen of the underlying Carlile Shale is type III. Because of converging evolution pathways with increasing maturity, the lower maturity cores (wells 1 and 2) are far better indicators of original OM type. It should be noted that samples from the B-chalk interval in wells 1 and 2 (Figure 5A, B) are not really chalks but marls with high

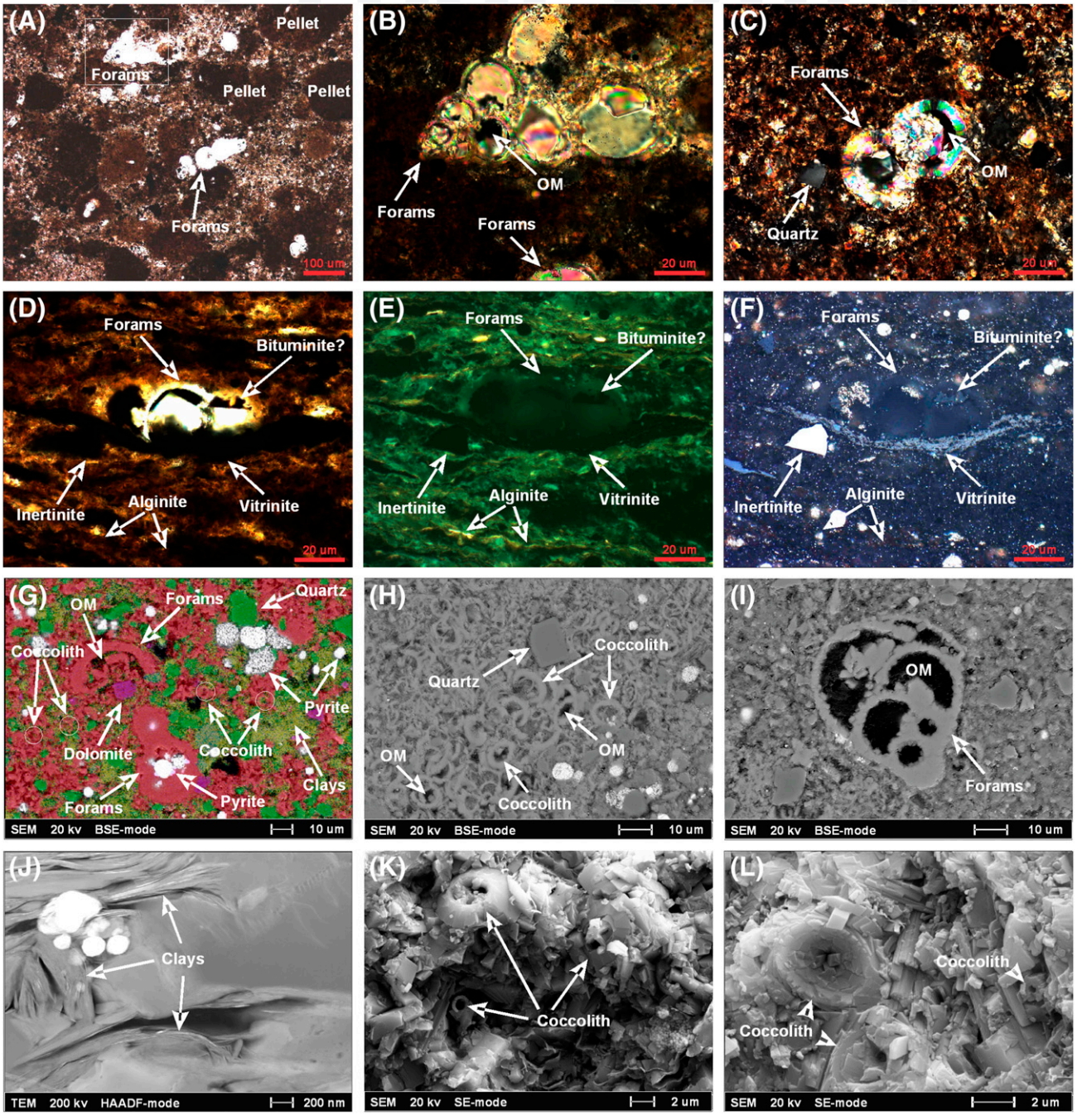

Figure 3. Photomicrographs showing petrographic features. (A) Sample G014905 from the A-marl interval of well 4; under polarized light, micritic calcite matrix, calcareous pellets, and foraminifera (forams) are the principal components (52 wt. % carbonate; oil saturation index [*OSI*] = 56 mg of hydrocarbons [HC]/g TOC). The rectangular marked area is magnified as seen in (B). (B) Under cross-polarized light, sparry calcite filling the tests of foraminifera. (C) Sample G014908 from the C-marl interval of well 4; under cross-polarized light, sparry calcite partly filling the tests of foraminifera (48 wt. % carbonate; *OSI* = 46 mg HC/g *TOC*). (D) Sample G014867 from the B-chalk interval of well 1; under polarized light, sparry calcite partly filling the foraminifera; 52 wt. % carbonate (*OSI* = 28 mg HC/g *TOC*). The same area is shown in as seen in (E, F). (E) Under fluorescent light, alginites are abundant. (F) Under reflected white light, foraminiferal tests are partly filled by organic matter (OM) (bituminite?). (G) Sample G014908 from the C-marl interval of well 4 via energy-dispersive spectroscopy element mapping. Calcite in red is the dominant mineral with abundant coccolith fragments, quartz in green is of detrital origin, clays in yellow are finely dispersed, and dolomite in magenta is scarce (48 wt. % carbonate; *OSI* = 46 mg HC/g *TOC*). (H) Sample G014874 from the C-marl interval of well 1 via backscattered electron (BSE) image; OM filling the chambers of coccolith (38 wt. %

TOC content (6.89–10.30 wt. %) (Tables S1 and S2, supplementary material available as AAPG Datashare XX at www.aapg.org/datashare). Brightly fluorescing alginites are abundant in these samples (Figure 3E).

The T_{max}–*HI* diagram proposed by Espitalié et al. (1984) takes maturity into account and yields overall similar results for the sample set with respect to kerogen typing (Figure 6). As seen in the pseudo Van Krevelen diagram (Figure 5), the alginite-rich samples from the B-chalk interval exhibit the highest kerogen quality of all type II kerogen containing Niobrara samples (Figure 6A, B).

The majority of the source rock samples exhibit T_{max} values between 430°C and 465°C (806°F and 869°F) (Figure 6), characteristic for catagenetic maturity levels. Values of T_{max} at approximately 440°C (~824°F) for samples in wells 1 and 2 are indicative for early–peak oil window maturities, whereas T_{max} values at approximately 450°C (~842°F) for samples in well 3 and 4 are, in connection with a clearly depleted HC potential (Table 2), indicative of late oil–wet gas window maturities. Well 5 contains the most mature samples with an average T_{max} value of 458°C (856°F) (Table 2) corresponding to end of oil window. The *HI* values gradually decrease from well 1 to well 5 (Figure 6; Table 2). It was recently proposed for the Barnett Shale (Lewan and Pawlewicz, 2017) and the Posidonia Shale (Stock et al., 2017) that *HI* trends offer a better proxy for maturity than the T_{max} trends. This also appears to be the case in the Niobrara Formation on first glance (Table 2). However, the Niobrara Formation is very heterogeneous and contains type II samples of very different quality reflected in differences in *HI* for similar maturity levels (Figures 5, 6). The application of *HI* as the sole maturity proxy should be treated with caution.

Open-system Py-GC was conducted for source rock samples from well 1 to further characterize kerogen types on a molecular level (aromaticity and aliphaticity, phenol abundance, and sulfur content) using the triangular plots of Larter (1984) (Figure 7) and Eglinton et al. (1990) (Figure 8). In accordance with previous Rock-Eval results (Figures 5A, 6A), all samples from the Smoky Hill Member (and Sharon Springs Member) plot very close to each other in the organofacies fields characteristic of type II marine OM. The B-chalk source rock kerogens are the samples most enriched in aliphatic moieties (n-$C_{8:1}$ in Figure 7 and n-$C_{9:1}$ in Figure 8) but do not quite reach aliphaticity levels typically observed for homogeneous type I alginites. In contrast, aromatic moieties (*m,p*-xylene in Figure 7 and *o*-xylene in Figure 8) dominate kerogens of samples from the Fort Hays Member (type IV) and Carlile Shale (type III). Pyrolysates of all samples are neither enriched in phenolic compounds (Figure 7), indicating an absence of terrestrial higher land plant–derived OM, nor in sulfur compounds (Figure 8), which is possibly because of their mid–oil window maturity levels because sulfur bonds within the kerogen network are known to be depleted very early during oil generation.

Overall, the majority of source rock samples (carbonate <70 wt. %) are classified as containing marine type II kerogen, whereas oil generation potential correlates with aliphaticity of the kerogen. Organic-rich marls from the B-chalk interval are of highest quality, whereas the organic-poor (<2.5 wt. % *TOC*) types III and IV samples from the Fort Hays Member and Carlile Shale exhibit lowest quality.

Oil Retention in Source Rocks

A reliable approach of quantifying the total amount of oil in place is prerequisite to assess oil retention characteristics of shales. Rock-Eval S_1 (Peters, 1986)

Figure 3. Continued. carbonate; *OSI* = 80 mg HC/g *TOC*). (I) Sample G014875 from the C-marl interval of well 1 via BSE image; OM and semieuhedral calcite crystals are filling the tests of foraminifera (25 wt. % carbonate; *OSI* = 72 mg HC/g *TOC*). (J) Sample G014905 from the A-marl interval of well 4 via transmission electron microscopy (TEM) image (high-angle annular dark-field [HAADF] imaging mode; Z-contrast); deformed clay minerals showing features of detrital origin (52 wt. % carbonate; *OSI* = 56 mg HC/g *TOC*). (K) Sample G015821 from the A-chalk interval of well 3 via secondary electron (SE) image; porous coccolith fragments are abundant (88 wt. % carbonate; *OSI* = 546 mg HC/g *TOC*). (L) Sample G015829 from the B-chalk interval of well 3 via SE image; porous coccolith fragments are abundant (93 wt. % carbonate; *OSI* = 382 mg HC/g *TOC*). Notably, photomicrographs were mainly selected here to show fossils and may not lithological representative of individual samples.

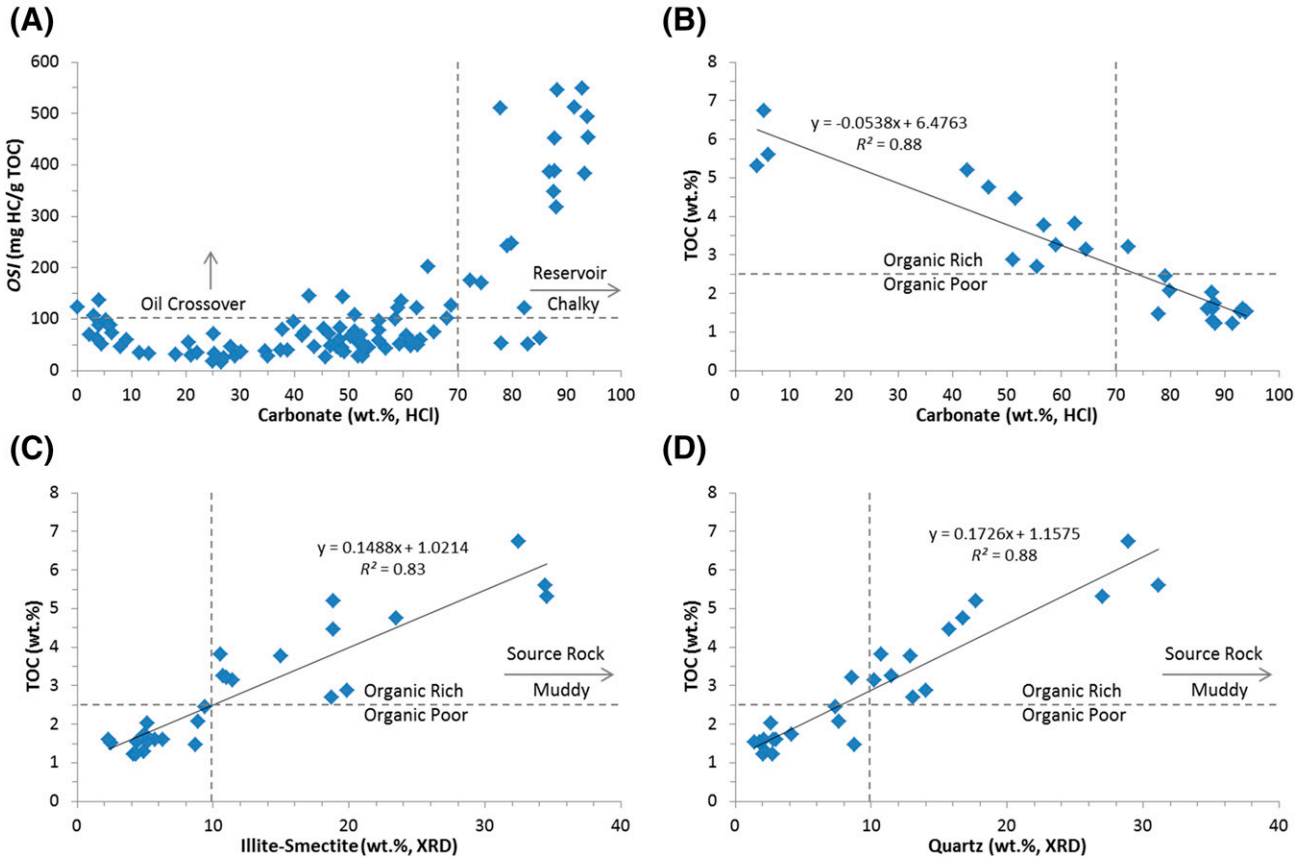

Figure 4. Crossplots of (A) oil saturation index (*OSI* = [S_1/total organic carbon (*TOC*)] × 100) versus carbonate content, (B) *TOC* versus carbonate content in well 3, (C) *TOC* versus illite–smectite content in well 3, and (D) *TOC* versus quartz content in well 3. HC = hydrocarbon; R^2 = xxx; XRD = x-ray diffraction.

and solvent extract yields (Claypool and Reed, 1976) are traditionally used for evaluating the amount of oil retained in rock samples. Nevertheless, neither the S_1 nor the extract yields can fully represent the molecular weight range of retained oil (Larter, 1988) because heavy compounds (>C_{17}) are not fully mobilized under pyrolysis conditions (Han et al., 2015), and compounds less than C_{15} HCs are lost during solvent evaporation (Peters et al., 2005). By applying comparative Rock-Eval pyrolysis (Delvaux et al., 1990) (i.e., comparing the pyrolysis results before and after solvent extraction), the total amount of retained oil can be quantified (Han et al., 2015) as follows: total oil = $S_{1whole\ rock} + S_{2whole\ rock} - S_{2extracted\ rock}$.

An excellent correlation exists for the sample set between calculated total oil yields and both S_1 and

Table 1. Major Niobrara Lithologies

Lithology	Carbonate, wt. %	Siliciclastics, wt. %	Rock Type	*TOC* Richness
Chalk	>85	<15	Reservoir	Organic poor
Marly chalk	85–70	15–30	Reservoir	↕
Marl	70–30	30–70	Source rock (reservoir?)	
Marly mudstone	30–15	70–85	Source rock	
Mudstone	<15	>85	Source rock	Organic rich

The major lithology types are empirically determined according to Tables S1–S5 (supplementary material available as AAPG Datashare XX at www.aapg.org/datashare), and the percentage of siliciclastic detritus (such as quartz, feldspar, clay minerals, mica, etc.) is relative to the content of carbonate (weight percent).
Abbreviation: *TOC* = total organic carbon (wt. %).

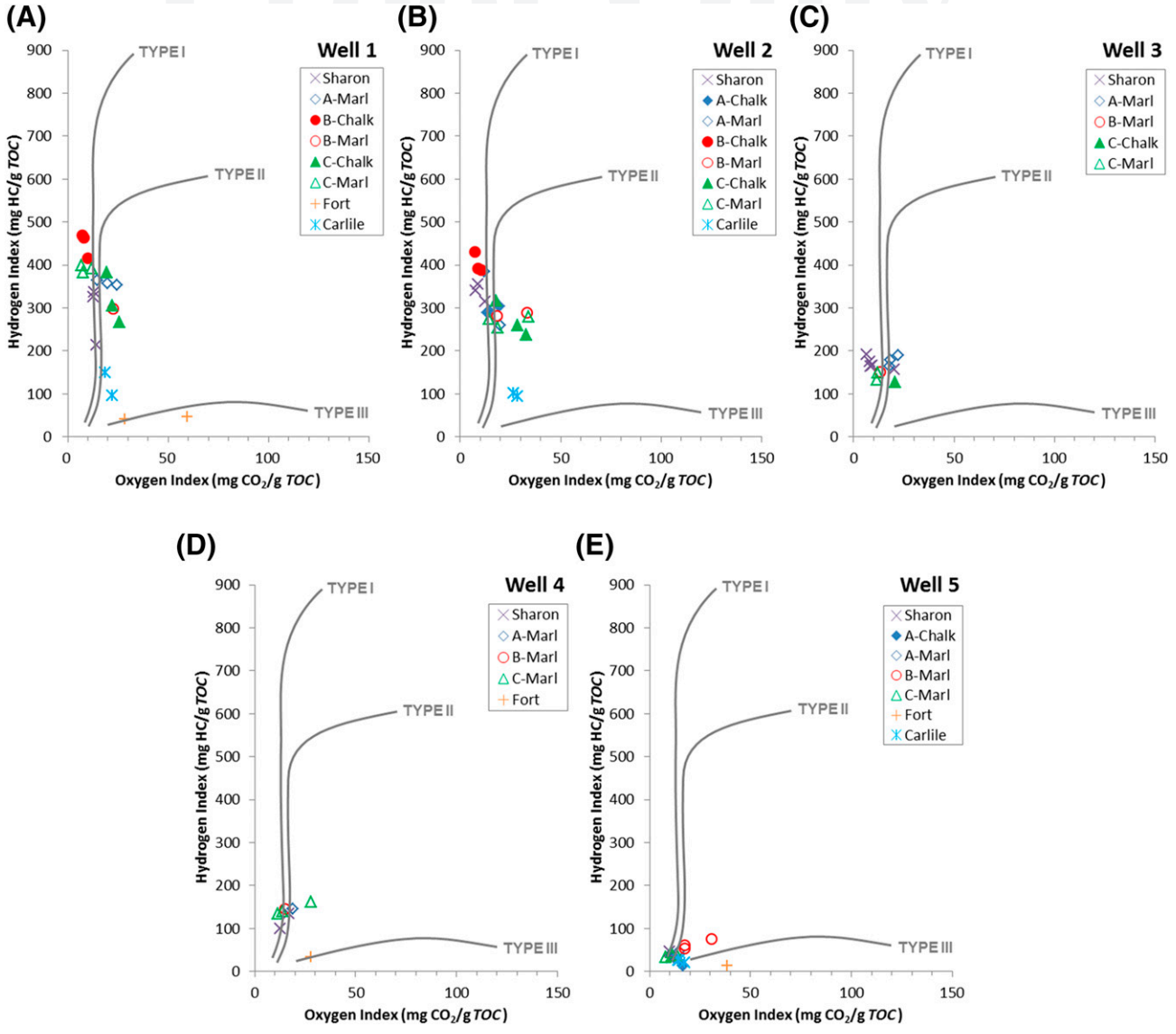

Figure 5. Pseudo Van Krevelen diagrams of hydrogen index versus oxygen index for source rock samples (carbonate <70 wt.%) in five studied wells. (A–E) Wells 1–5, respectively. Modified from Espitalié et al. (1977). HC = hydrocarbon; TOC = total organic carbon.

solvent extract yields (Figure 9). Because S_1 always shows a better correlation coefficient with the total oil ($R^2 > 0.88$) than extract yields ($R^2 < 0.87$), S_1 has been used in the ensuing discussions to act as a screening tool for the retained total oil amount. Because a similar maturity (T_{max}) was obtained for wells 1 and 2 and wells 3 and 4, respectively (Table 2), samples from these wells are plotted together. With increasing maturity, the proportion of S_1 to total oil gradually increases from 46% (0.46 = 1/2.1650) in wells 1 and 2 (Figure 9A) to 72% (0.72 = 1/1.3979) in wells 3 and 4 (Figure 9B) and 81% (0.81 = 1/1.2298) in well 5 (Figure 9C). This reflects increasing proportions of volatile HCs in the calculated total oil amount, whereas C_{1-5} gas HCs that were lost during sampling (Larter, 1988; Sandvik et al., 1992) are not accounted for here.

In general, the higher the OM richness, the higher the amount of retained oil (Baker, 1962; Tissot et al., 1971; Stainforth and Reinders, 1990; Pepper, 1991). Accordingly, oil retention in the source rock samples seems to be controlled primarily by OM richness (Figure 10). However, the organic-rich B-chalk samples fall off the general trend and retain much less oil (S_1) than the other samples in wells 1 and 2 (Figure 10A). No source rock samples

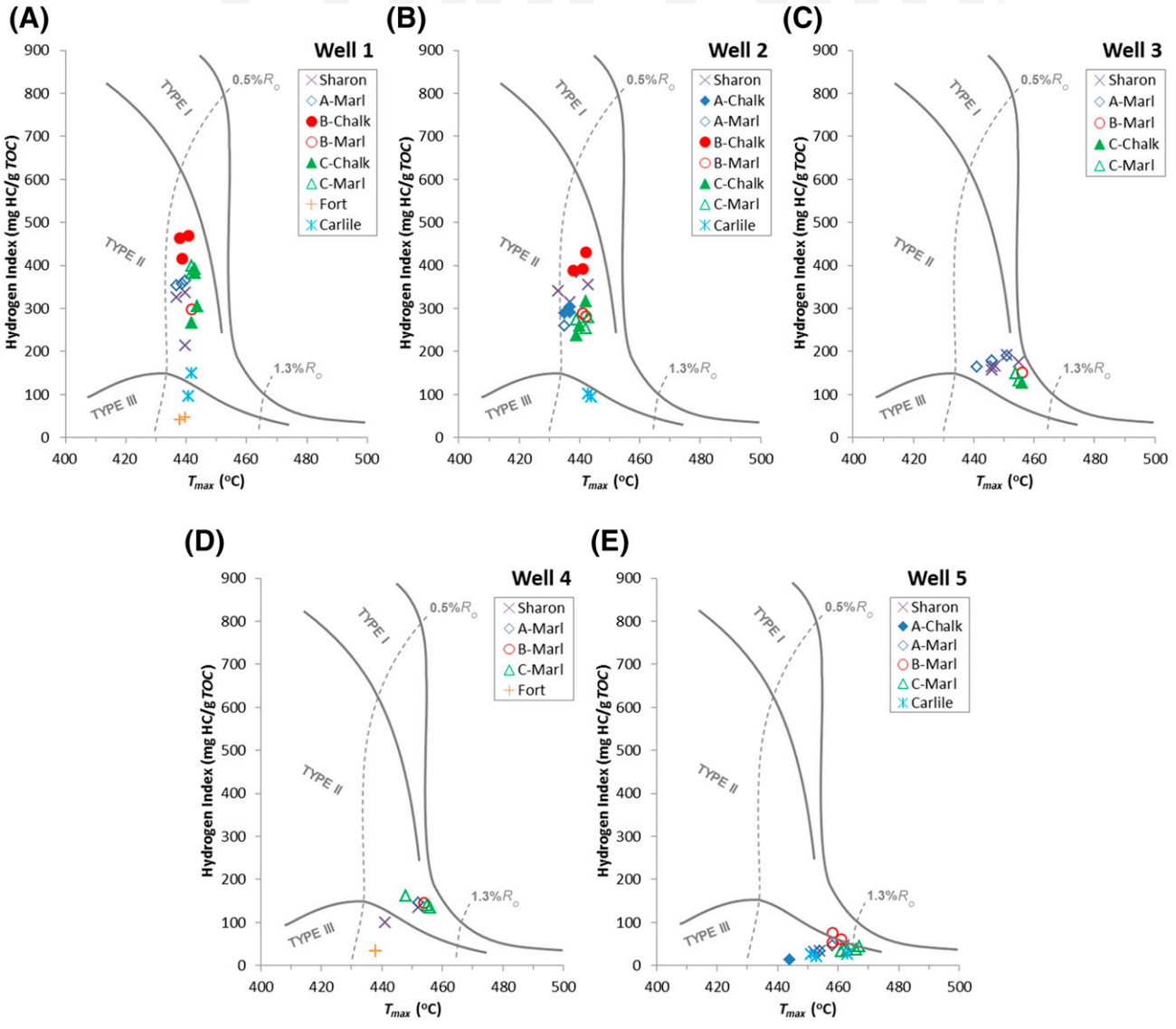

Figure 6. Kerogen typing diagrams of hydrogen index versus the temperature at the maximum rate of petroleum generation by Rock-Eval pyrolysis (T_{max}) for source rock samples (carbonate <70 wt.%) in five studied wells. (A–E) Wells 1–5, respectively. Modified from Espitalié et al. (1984). HC = hydrocarbon; R_o = vitrinite reflectance.

are selected from the B-chalk interval in the other wells (Figure 10B, C).

Based on previous studies, the retention of oil in source rock is controlled mainly by the sorption capacity of its OM (Baker, 1962; Tissot et al., 1971; Stainforth and Reinders, 1990; Pepper, 1991), and a sorption threshold of 100 mg HC/g *TOC* was proposed, irrespective of kerogen type and thermal maturity (Sandvik et al., 1992; Jarvie, 2012). Some samples from wells 1 and 2 (Figure 10A) and wells 3 and 4 (Figure 10B) exceed this threshold value. For example, sample G015824 (65 wt. % carbonate; Table S3, supplementary material available as AAPG Datashare XX at www.aapg.org/datashare) shows a distinct oil crossover and has the highest *OSI* value (202 mg/g *TOC*) among all source rock samples (Figure 10B). Although being classified as a source rock (carbonate <70 wt. %), this and other marl samples showing oil crossovers have reservoir characteristics as well. In contrast, and because of higher maturity, none of the samples from well 5 show oil crossover effects (Figure 10C), and S_1 values are lower (<3 mg/g) than those of wells 1 and 2 (<7 mg/g) (Figure 10A) and wells 3 and 4 (<8 mg/g) (Figure 10B) for comparable *TOC* contents.

Table 2. Averaged Total Organic Carbon and Rock-Eval Data for Nonextracted Source Rock Samples (Carbonate <70 wt. %)

Well Name	Sample Number	Carbonate, wt. %	*TOC*, wt. %	S_1 mg HC/g	S_2 mg HC/g	T_{max}, °C	*OSI* mg HC/g TOC	*HI* mg HC/g TOC
Well 1	20	40	3.97	2.36	14.74	441	60	303
Well 2	21	40	4.46	3.10	14.43	440	73	292
Well 3	12	42	4.30	4.36	7.03	450	102	162
Well 4	8	33	3.17	1.74	4.15	450	54	124
Well 5	17	37	3.13	1.51	1.20	458	47	37

Before Soxhlet extraction, and samples with more than 70 wt. % carbonate are not included.
Abbreviations: *HI* = hydrogen index ([S_2/*TOC*] × 100; mg HC/g *TOC*); *OSI* = oil saturation index ([S_1/*TOC*] × 100, mg HC/g *TOC*); S_1 = the vaporizable hydrocarbons yield at nominal temperatures at 300°C (572°F); S_2 = the yield of pyrolysis products generated at a temperature up to 650°C (1202°F); T_{max} = the temperature at maximum rate of petroleum generation by Rock-Eval pyrolysis (°C [°F]); *TOC* = total organic carbon (wt. %).

To reveal the control of thermal maturity on retention, the *OSI* values of Niobrara source rock samples are plotted against their T_{max} values (Figure 11). In general, the Niobrara source rock samples fall on the maturity evolution pathway earlier defined for the Barnett and Posidonia Shales (Han et al., 2017). Because our Niobrara sample set does not contain any immature source rocks with T_{max} values lower than 430°C (<806°F), data collected from Rice (1984) and Thul (2012) are plotted in Figure 11. However, samples with reservoir characteristic may be included in their sample set as well and thus exhibit *OSI* values greater than those of typical marine source rocks. In general, the *OSI* first increases in the oil window and subsequently decreases once the threshold value (100 mg HC/g *TOC*) is exceeded at a T_{max} of approximately 445°C (~833°F). For the type II OM-containing Barnett Shale, this temperature is equivalent to thermal stress levels of 0.85 R_c % according to Jarvie et al. (2007) as follows: R_c % = 0.018 × T_{max} – 7.16. Even with allowing for variability in kinetics, this maturity level (0.85 R_c %) is obviously not large enough for the secondary cracking of oil into gas, which was reported to start at approximately 1.2% R_o in the Posidonia Shale (Dieckmann et al., 1998) and at 1.1% R_o (Hill et al., 2007) or 1.5% R_o (Lewan and Pawlewicz, 2017) in the Barnett Shale.

Some samples clearly exhibit higher *OSI* values than the majority of source rock samples that define the generalized curve (Figure 11). In the Barnett and Posidonia Shales, samples with exceptional reservoir potential are characterized by the presence of porous fossil fragments, namely, sponge spicules (Han et al., 2015) and coccolith (Han et al., 2016 accepted), respectively. These high *OSI* samples constitute the sweets spots that are keenly sought during exploration. In the Niobrara Formation, the exceptional source rock samples have carbonate between 49 and 69 wt. % and are characterized by relative abundant calcite fossils (described in detail in the next section). Nevertheless, the main targets (i.e., sweet spots) are the chalk reservoir rocks discussed in the next section.

To summarize this part, the retention of oil in source rock samples (carbonate <70 wt. %) from the Niobrara Formation is controlled by OM properties (i.e., *TOC*, kerogen type, and thermal maturity). The higher the richness in OM (*TOC*), the higher is the amount of retained oil through sorption.

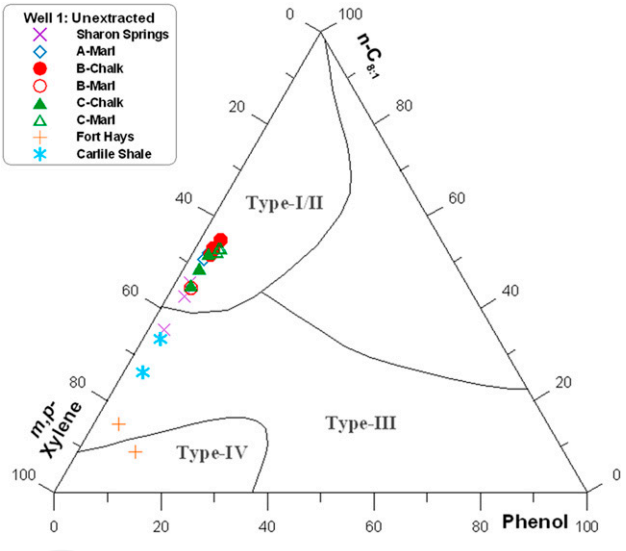

Figure 7. Ternary diagram showing kerogen types and the relative abundance of *m,p*-xylene, n-$C_{8:1}$ and phenol in Niobrara source rock samples. Modified from Larter (1984).

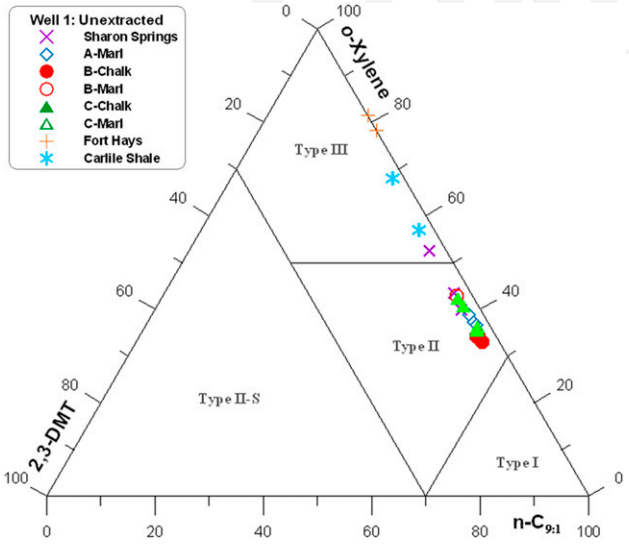

Figure 8. Ternary diagram showing kerogen types and the relative abundance of dimethylthiophene (2,3-DMT), *o*-xylene, and n-$C_{9:1}$ in Niobrara source rock samples, modified from Eglinton et al. (1990). II-S = xxx. Q:58

More aliphatic type II samples show different retention behavior than the more aromatic types III and IV samples. For instance, and for a given OM richness (*TOC*), the most aliphatic source rock samples from the B-chalk interval retain much less oil (S_1) through sorption than samples from the other intervals. With increasing maturity, the oil retention capacity (expressed in $OSI = S_1/TOC \times 100$) of Niobrara source rock samples first increases until a T_{max} of approximately 445°C (~833°F) and then decreases.

Organic Pores in Source Rocks

It is widely accepted that organic pores owe their origin to the thermal cracking of kerogen and bitumen in the sense of extractable OM (Loucks et al., 2009; Bernard et al., 2012b, 2013; Curtis et al., 2012; Mastalerz et al., 2013; Romero-Sarmiento et al., 2013; Pommer and Milliken, 2015; Ko et al., 2016; Han et al., 2017). Clearly, the maturity level does not vary significantly in the least mature well 1 (T_{max} 437°C–444°C [819–831°C]) (Figure 6A). However, nano-size pores are well developed within OM from the B chalk of this well but not common in other intervals (Figure 12). The organic pores observed in the spatially isolated organic particles from the B chalk have a sponge-like character (Figure 12E–H). Except for the B-chalk samples, there is no visible (>2 nm) pore observed in the elongated organic particles of likely detrital origin (Figure 12A, B, I, J) even after a longer EDXS scanning time (Figure 12L). According to Han et al. (2017) it can be inferred that the thermal breakdown of OM and the release of HCs leads to pore formation in the OM, that is, the occurrence of organic pores Q:35

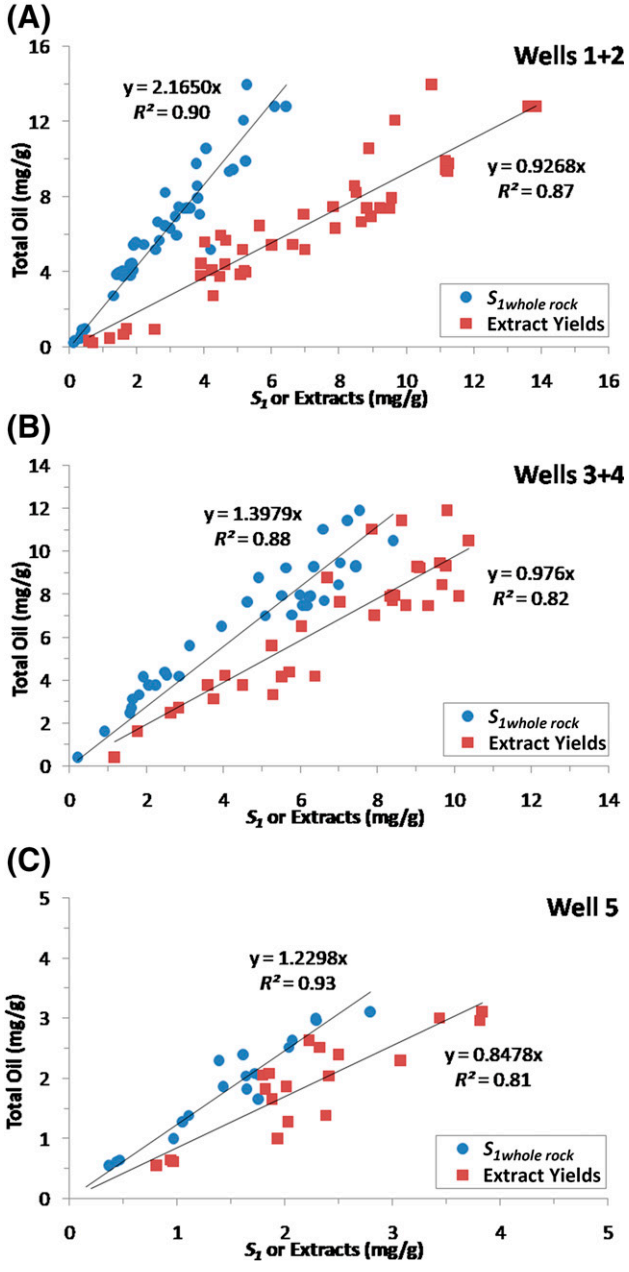

Figure 9. The S_1 values of original pulverized samples and solvent extract yields versus the amounts of calculated total oil (total oil = $S_{1whole\ rock} + S_{2whole\ rock} - S_{2extracted\ rock}$) in (A) wells 1 and 2, (B) wells 3 and 4, and (C) well 5. R^2 = xxx. Q:59

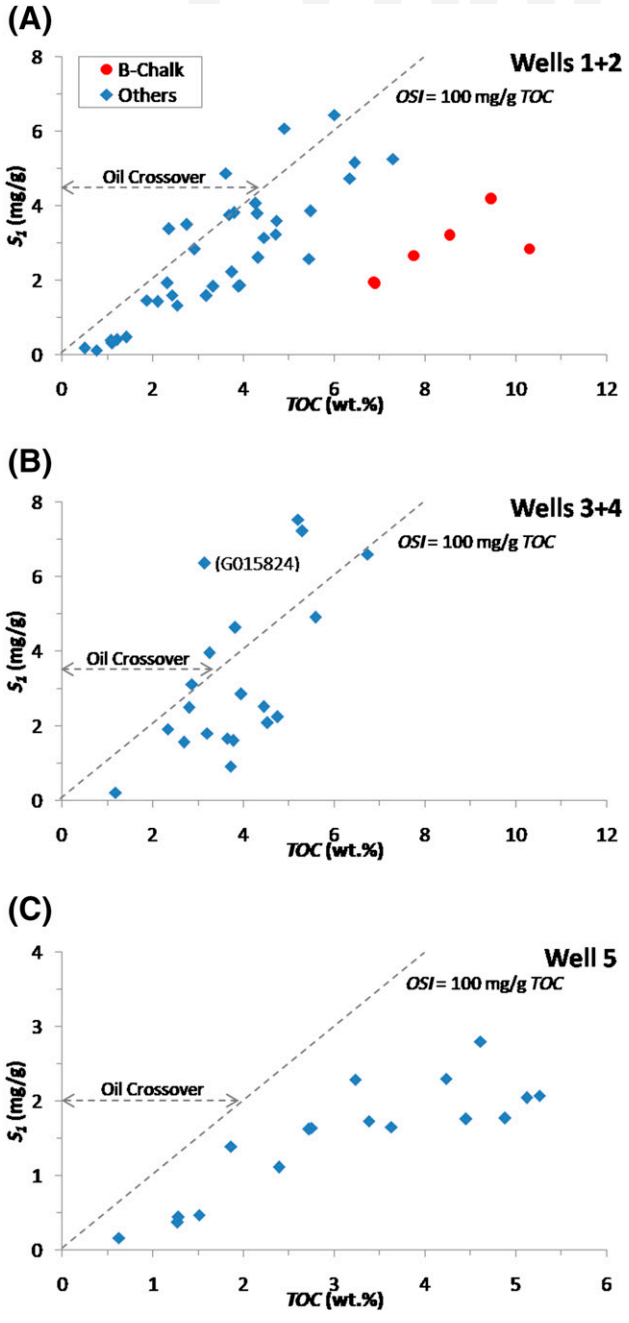

Figure 10. Controls on oil retention in source rock samples (carbonate <70 wt. %) are revealed by plotting S_1 versus total organic carbon (*TOC*) content in (A) wells 1 and 2, (B) wells 3 and 4, and (C) well 5. *OSI* = oil saturation index.

can be treated as a tracer of nascent or ongoing petroleum generation and expulsion. Assuming this hypothesis is correct, the occurrence of organic pores indicates a depleted oil retention capacity of the host kerogen. In line with that, oil retention capacity of B-chalk samples is lower than that of other source rock samples (Figure 11).

It is noteworthy that brightly fluorescing alginites (Figure 3E) occur in the samples that are richest in OM (6.89–10.30 wt. % *TOC*) (Tables S1 and S2, supplementary material available as AAPG Datashare XX at www.aapg.org/datashare), have the highest *HI*s (Figures 5, 6), and are most aliphatic (Figures 7, 8). Because the OM in the B chalk is therefore compositionally distinct, it is to be expected that its response to thermal cracking might also be distinctive. Accordingly, the formation of organic pores in this OM is one such characteristic that can be expected to follow a different pattern. Indeed, the kerogen-like OM in these B-chalk marls is porous in contrast to those from other intervals in the least mature well 1. No TEM-visible (>2 nm) pores are developed within the OM stringers from other intervals in well 2 (Figure 13).

In addition to the organic particles occurring as elongated stringers, others with a smeared, filmy appearance were documented (Figure 12D, K). In most cases, the filmy OM is hosted in mineral pores whose straight boundaries likely correspond to coccolith plate edges. This OM is extremely porous with bubble-like appearance. These morphological features suggest that the filmy OM may represent relics of redistributed bitumen. Their presence in mineral pores indicates an enhanced reservoir potential of the two samples G014865 and G014872, whereas it is hard to say whether it is producible oil or not. Both samples exhibit relatively high *OSI* values (102 and 97 mg HC/g *TOC*, respectively) and plot above the generalized *OSI* evolution curve (Figure 11). In other words, they are defined as source rock samples (carbonate <70 wt. %), but they nevertheless exhibit some reservoir potential. Nevertheless, the fact remains that the main targets (i.e., sweet spots) are the chalk intervals as discussed in the next section.

RESERVOIR ROCK CHARACTERISTICS IN WELL 3

According to previous discussions, chalk and marly chalk (Table 1) with carbonate contents greater than 70 wt. % are promising reservoir rocks exhibiting *OSI* values greater than 100 mg HC/g *TOC* (Figure 4A). Of the 98 analyzed samples (Tables S1–S5, supplementary material available as AAPG Datashare XX at www.aapg.org/datashare), 20 can be classified as reservoir rocks. Of those core samples,

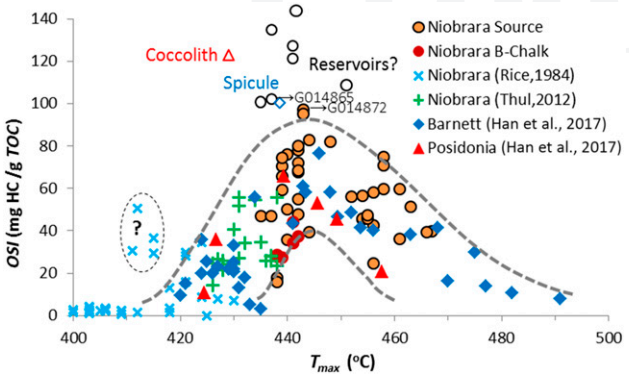

Figure 11. Total organic carbon (*TOC*) normalized oil retention capacity (oil saturation index [*OSI*]) as a function of the temperature at the maximum rate of petroleum generation by Rock-Eval pyrolysis (T_{max}) in the Barnett Shale, Posidonia Shale, and Niobrara Formation. The evolution curves are taken from Han et al. (2017) as well as the data of Barnett Shale (diamonds) and Posidonia Shale (triangles). Samples with an *OSI* greater than 100 mg of hydrocarbons (HC)/g *TOC* are represented by empty patterns. Only the source rock samples (carbonate <70 wt.%) from the Niobrara Formation are plotted (circles). Samples from the Sharon Springs Member of Pierre Shale and the Carlile Shale are not shown. Data from Rice (1984) and Thul (2012) are plotted to show the relationship to immature Niobrara source rocks. Sample G015824 is plotted beyond the plot because of its high *OSI* value (202 mg HC/g *TOC*). Samples G014865 and G014872 are shown in Figure 12 C–D and I–L, respectively. Q:61

15 can be found in well 3 and were thus selected to characterize the chalk reservoirs in the Niobrara shale oil play (Table S3, supplementary material available as AAPG Datashare XX at www.aapg.org/datashare). In the following, source rock samples from well 3 are shown in comparison to the reservoir samples because there is no clear lithological boundary between reservoir and source rock samples anyhow (Table 1).

Geochemical Log of Well 3

A geochemical depth profile of well 3 is shown in Figure 14. Significant heterogeneities between the chalk and marl intervals are revealed through XRD. The A and B chalks are almost exclusively composed of calcite (>85 wt. %), which is the empirical criterion that is used to define the chalk lithology (Table 1). Because of low-density sampling, we will not focus on the C-chalk interval and the Fort Hays Member.

In comparison to the chalks, the A, B, and C marls contain higher amounts of siliciclastic minerals (e.g., illite–smectite mixed layers [IS] clays and quartz [Figure 14]). As previously discussed, a positive correlation of quartz and IS-clay mineral contents indicates a common detrital origin (Figure 2C). Variations in siliciclastic flux therefore account for the rhythmic bedding of chalk-marl intervals in which autochthonous or allochthonous component abundance is inversely related. Thus, changes in illite–smectite and quartz contents are in contrast to changes in calcite content (Figure 14). Interestingly, and as previously discussed (Figure 4B–D), *TOC* is positively correlated with quartz and IS-clay mineral content and thus also inversely proportional to calcite contents (Figure 14). A likely explanation for low *TOC* is dilution by rapid carbonate sedimentation (Frébourg et al., 2016; Denne et al., 2016). Q:36 Q:37 Therefore, *TOC* can be as high as 7 wt. % in the Sharon Springs Member, less than 5 wt. % in the marls, and lowest in the chalks (*TOC* < 2.5 wt. %). Volatile HCs (S_1) make up a high proportion of the in-place OM fraction in the organic-lean chalks. This is manifested in high *OSI* values (>300 mg HC/g *TOC*). The HC potential (S_2) evolves similarly to the *TOC* content leading to similar *HI* values between 100 and 200 mg HC/g *TOC* throughout the core. In contrast, *OI* values and T_{max} are not stable. In A and B chalks, *OI* values are higher, and T_{max} values are lower than in the other intervals (Figure 14). Q:38 Q:39

Maturation and Intraformational Migration of Hydrocarbons in Well 3

For source rock samples (carbonate <70 wt. %) of well 3, T_{max} values average approximately at 450°C (~842°F) (Table 2). Reservoir samples from the A and B chalks exhibit much lower T_{max} values (i.e., 421°C –433°C [790°F–811°F] and 437°C –446°C [819–835°F], respectively) (Figure 14). Clearly, besides being influenced by thermal stress, other factors such as the presence of heavy petroleum compounds might affect the T_{max} values in the A and B chalks. Q:40

It is well known that migration and emplacement of heavy petroleum compounds in reservoir rock intervals can result in anomalously low T_{max} values (Clementz, 1979; Peters, 1986; Jarvie, 2012; Han

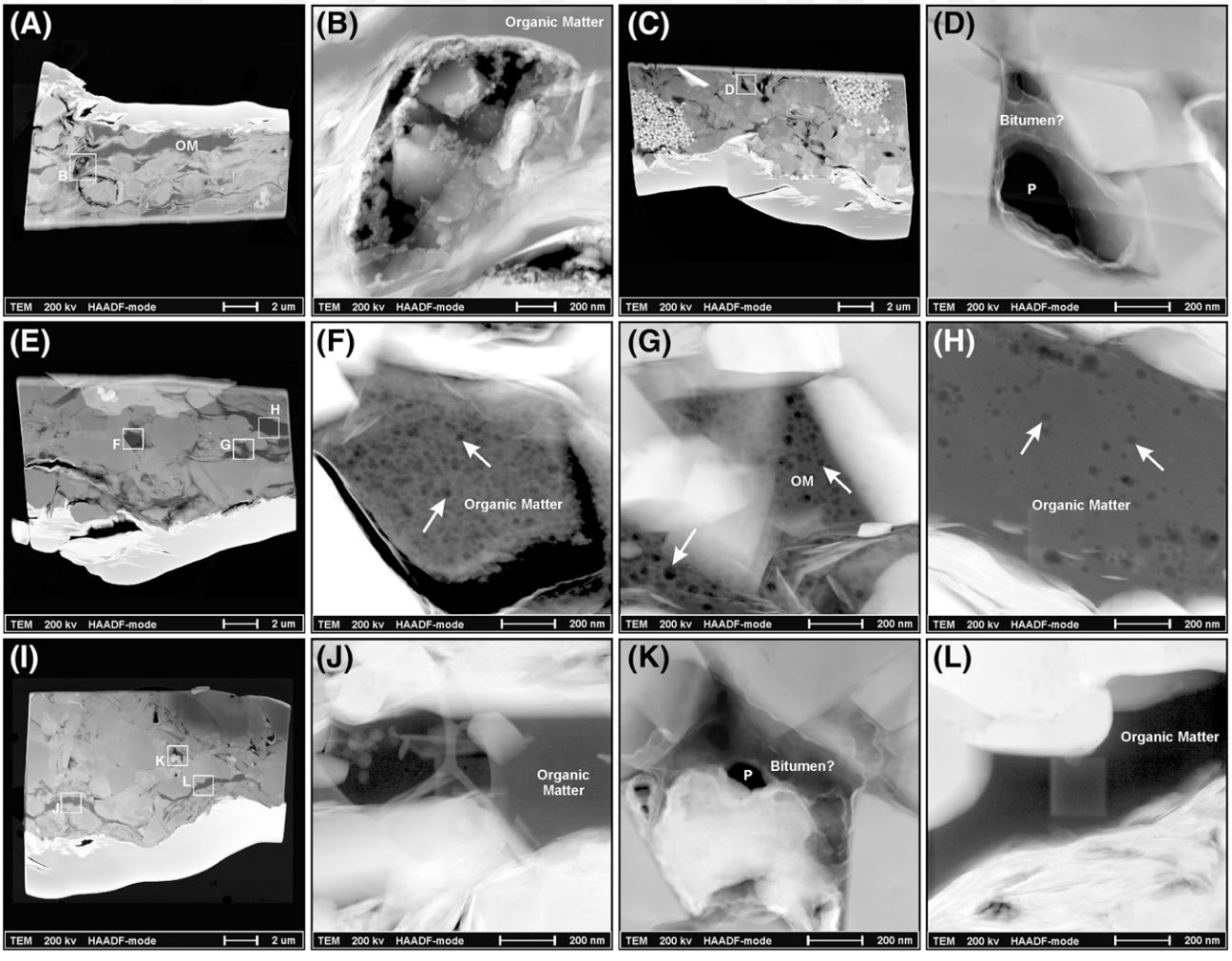

Figure 12. Transmission electron microscopy (TEM) images (high-angle annular dark-field [HAADF] mode; Z-contrast) showing organic pores (white arrow). Focused ion beam foils were extracted from source rock samples (carbonate <70 wt. %) from well 1. The rectangular marked areas are magnified in following figures. (A, B) Sample G014861 from the Sharon Springs Member (2 wt. % carbonate; oil saturation index [*OSI*] = 70 mg of hydrocarbons [HC]/g *TOC*); no TEM-visible (>2 nm) pores developed within the stringers of organic matter (OM). (C, D) Sample G014865 from the A-marl interval (68 wt. % carbonate; *OSI* = 102 mg HC/g *TOC*); bubble-like nanopores are observed in filmy OM of possible bitumen origin. Interparticle mineral pore (P) is partly occluded by those OMs. (E–H) Sample G014867 from the B-chalk interval (52 wt. % carbonate; *OSI* = 28 mg HC/g *TOC*); sponge-like nanopores are developed within the OM. (I–L) Sample G014872 from the C-chalk interval (55 wt. % carbonate; *OSI* = 97 mg HC/g *TOC*), no TEM-visible (>2 nm) pores developed within the elongated OM stringers of possible detrital origin; only bubble-like nanopores are observed within the filmy OM of possible bitumen origin. The rectangular area as seen in (L) is still not porous after energy-dispersive x-ray spectroscopy scanning.

et al., 2015). To assess whether this occurs here, comparative Rock-Eval pyrolysis (Delvaux et al., 1990) was performed on samples both before and after solvent extraction. Typical pyrolysis traces for samples from the chalk and marl intervals are shown in Figure 15. After solvent extraction of the chalk samples (Figure 15A), S_2 peak areas significantly decrease, whereas peak shape is lower in height and shorter in width (red lines). In addition, a significant shift of the T_{max} to higher values can be observed. This shift is only very subtle for marl samples (Figure 15B). Here, the S_2 peak shapes are approximately similar before and after solvent extraction, with the exception of the removal of minor "pre-shoulders."

As reported for an oil-mature Barnett Shale core (Han et al., 2015), it is very likely that petroleum migrated into the chalk intervals, leading to a shift of high to low T_{max} values. For instance, after solvent extraction, a significant depletion of *TOC* content (29–41 wt. %) occurs for samples from the A and B

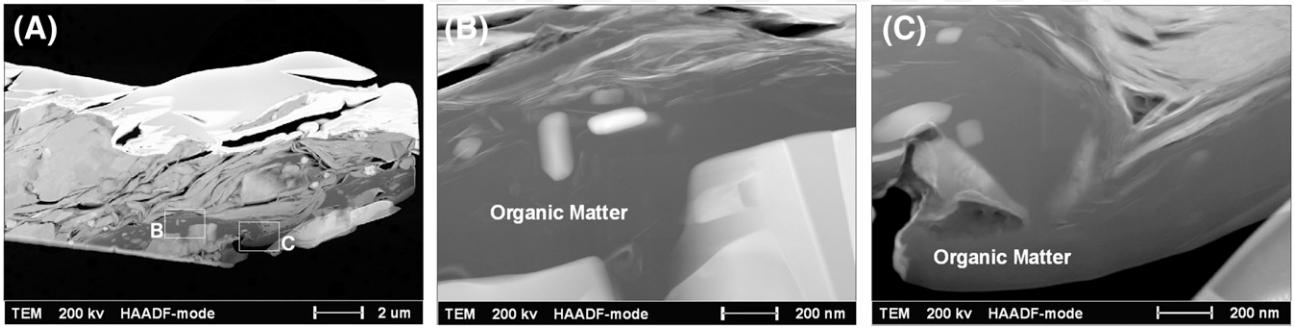

Figure 13. Transmission electron microscopy (TEM) images (high-angle annular dark-field [HAADF] mode; Z-contrast) of a focused ion beam foil extracted from sample G014887 from the A-marl interval of well 2. The rectangular marked areas in (A) are magnified as seen in (B) and (C), respectively. No TEM-visible (>2 nm) pores are developed within the organic matter stringers (52 wt. % carbonate; *OSI* = 70 mg of hydrocarbons per gram of total organic carbon).

chalks in well 3 (Table S3, supplementary material available as AAPG Datashare XX at www.aapg.org/datashare). In line with that, averaged *OSI* values are extremely high (>445 mg HC/g *TOC*, Table 3). It is highly improbable that such huge quantities of removable oil in A and B chalks could have originated from the indigenous OM, especially when taking *HI* values of samples from the less mature wells 1 and 2 into consideration (<450 mg HC/g *TOC*) (Table 3). As mentioned above, the gradual decrease of *HI* going from well 1 to well 5 (Table 2) is likely a result of thermal degradation. Comparing *HI* values of A- and B-chalk samples from well 2 to those of well 3 (Table 3), it becomes clear that their difference (154 and 229 mg HC/g *TOC*, respectively) is obviously lower than the corresponding increase in *OSI* (381 and 408 mg HC/g *TOC*, respectively). Thus, more HCs are present than could have been generated from their initial OM. Furthermore, the assumed initial HC generation potential for chalks of well 3 represents an overestimation when taking into account the samples from the A-chalk interval in wells 1 and 2 are interbedded organic-rich marls, but those of well 3 are true chalks with likely very low generation potential at immature stages. The same applies to the B chalk.

To keep things simple, we used (defined) the sum of the volatile HCs (S_1) and pyrolysate yield (S_2) normalized to *TOC* ($QI = [S_1 + S_2]/TOC \times 100$) as a quality index (*QI*) (Pepper and Corvi, 1995). In general, a decrease in *QI* with increasing maturity is a consequence of petroleum expulsion and primary migration out of source beds (Sykes and Snowdon, 2002). Nevertheless, *QI* values might also increase, indicating the presence or emplacement of migrated petroleum in a reservoir interval. With increasing maturity going from wells 1 and 2 to well 3, shale and marl intervals exhibit decreasing *QI* values, confirming source rock characteristics (Table 3). In contrast, *QI* values increase for the A, B, and C chalks of well 3, confirming reservoir characteristics. Thus, oil generated within the organic-rich layers very likely migrated into juxtaposed chalks where it was partly emplaced.

This migrated oil is mainly responsible for skewing the S_2 curve and lowering T_{max} in the chalk intervals (Figure 15A). As shown in Figure 15, the Rock-Eval apparatus is held at a nominal isothermal temperature of 300°C (572°F) for the first 3 min (actually 40°C [104°F] higher for the Rock-Eval 2 instrument). Some heavy-end oil compounds (beginning as early as n-C_{19+}) cannot be fully vaporized at those temperatures (Han et al., 2015) and thermally break down within the S_2 peak temperature range during programmed heating. For instance, 69%–77% and 57%–71% of the S_2 signal is lost after extraction for samples from the A and B chalks, respectively (Table S3, supplementary material available as AAPG Datashare XX at www.aapg.org/datashare), meaning that the major part of the pyrolysate in fact originates from heavy petroleum compounds and not from kerogen. Thus, the removal of extractable OM before pyrolysis is a prerequisite for the T_{max} value to reveal the maturity of kerogen.

For all solvent-extracted chalk samples, T_{max} values are significantly increased by more than 10°C [>50°F] (Table S3, supplementary material available as AAPG Datashare XX at www.aapg.org/datashare).

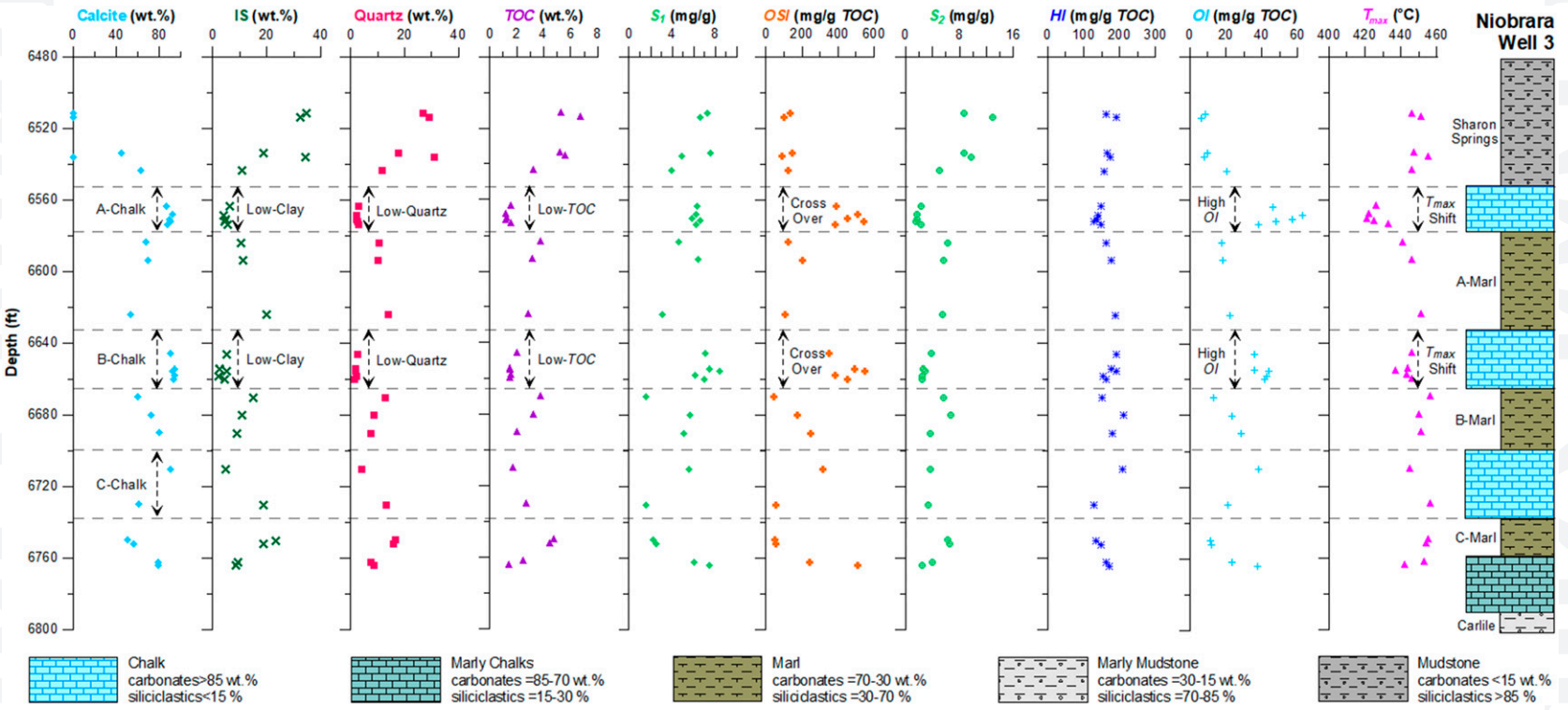

Figure 14. Geochemical depth profile of well 3. *HI* = hydrogen index ($S_2/TOC \times 100$); IS = illite–smectite mixed layers; *OI* = oxygen index ($S_3/TOC \times 100$), in which S_3 corresponds to the amount of CO_2 produced during pyrolysis of organic matter; *OSI* = oil saturation index ($S_1/TOC \times 100$); *TOC* = total organic carbon; S_1 = thermal extractable petroleum; S_2 = petroleum generated by pyrolysis; T_{max} = the temperature at maximum rate of petroleum generation by Rock-Eval pyrolysis.

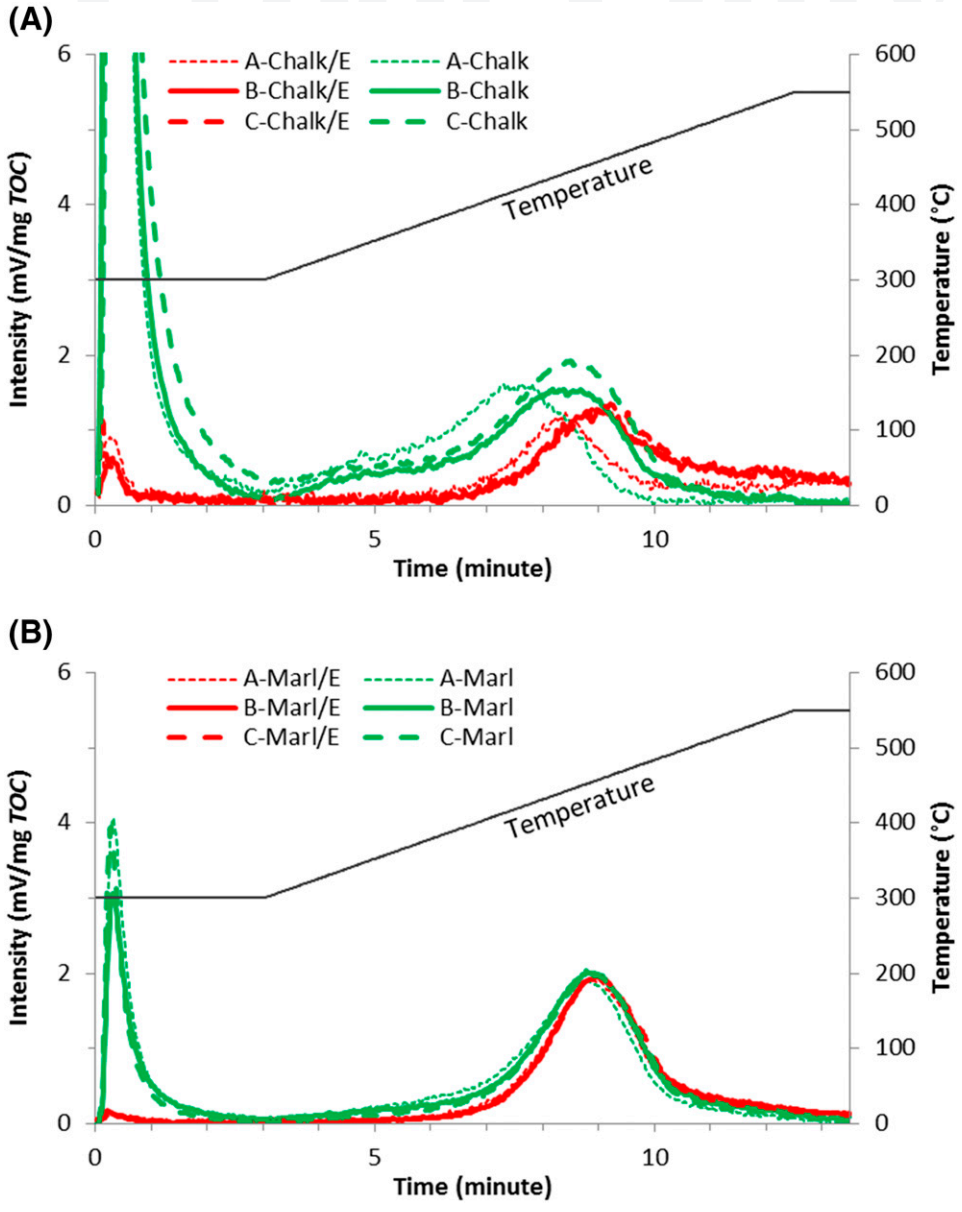

Figure 15. Rock-Eval traces of representative samples from (A) chalk intervals and (B) marl intervals before and after Soxhlet extraction. Extracted samples are indicated with an "E." Intensity (left y-axis) is normalized by dividing the initial signal intensity with the sample weight and total organic carbon (*TOC*). The right y-axis indicates the temperature program.

Extracted B-chalk sample T_{max} values (456–459°C [853–858°F]) are now similar to those of the adjacent marls (Table S3, supplementary material available as AAPG Datashare XX at www.aapg.org/datashare). However, T_{max} values of extracted A-chalk samples (432–449°C [810–840°F]) are still lower than those of all the other samples (Figure 16). Obviously, other factors might affect T_{max} values as a relatively stable maturity level should prevail throughout well 3.

Kerogen type can affect the T_{max} and many other geochemical parameters (Espitalié et al., 1984; Tissot and Welte, 1984; Espitalié, 1985). Using the *HI* for typing of OM in extracted well 3 samples, a more oxygen-rich (>20 mg CO_2/g *TOC*) and less hydrogen-rich kerogen (~50 mg HC/g *TOC*) remains in the A chalk compared to the other intervals (Figure 17A, B). Rock-Eval data of extracted A-chalk samples suggest type III kerogens. The particularly low values for the temperature at maximum rate of

Table 3. Rock-Eval Pyrolysis of Studied Wells

Rock-Eval	Name	Nr	Sharon	A Chalk	A Marl	B Chalk	B Marl	C Chalk	C Marl	Fort	Carlile
OSI (mg HC/g *TOC*)	Well 1	20	61	n.a.	79	30	78	83	82	26	31
	Well 2	23	106	76	114	37	101	55	95	n.a.	34
	Well 3	27	118	457	144	445	155	188	52	377	n.a.
HI (mg HC/g *TOC*)	Well 1	20	292	n.a.	358	450	299	318	391	43	122
	Well 2	23	337	294	325	404	285	271	269	n.a.	98
	Well 3	27	170	140	177	175	180	168	141	167	n.a.
QI (mg HC/g *TOC*)	Well 1	20	353	n.a.	438	479	377	401	474	69	153
	Well 2	23	443	371	439	441	386	326	364	n.a.	132
	Well 3	27	288	597	321	621	335	356	193	544	n.a.

Data are averages of all samples from each well before solvent extraction.
Abbreviations: *HI* = hydrogen index ([S_2/*TOC*] × 100; mg HC/g *TOC*); n.a. = not available; Nr = number of samples; *OSI* = oil saturation index ([S_1/*TOC*] × 100; mg HC/g *TOC*); *QI* = quality index ([$S_1 + S_2$]/*TOC* × 100; mg HC/g *TOC*).

petroleum generation by Rock-Eval pyrolysis detected on solvent-extracted samples of A-chalk samples in well 3 (Figure 16) seem to be related to the presence of a different kerogen type. Nevertheless, and taking data of wells 1 and 2 into consideration (Figures 5C, 6C), the majority of extracted samples from well 3 should be initially of a type II origin (Figure 17A, B).

Oil Retention and Pore Development in Reservoir Rocks

For nonreservoir rocks (carbonate <30 wt. %) in wells 3 and 4, *TOC* is positively correlated to S_1 (i.e., volatile oil is preferentially present in a sorbed state [Figure 18A]). For samples with more than 30 wt. % carbonate (reservoir rocks and source rocks with some reservoir characteristic), carbonate content shows a positive correlation with the amount of retained (stored) oil in all but one sample (Figure 18B). Here, most oil is likely stored as a fluid phase in pores of calcareous fossils rather than sorbed onto OM. As shown for the Barnett Shale (Han et al., 2015), for which the chambers of sponge spicules provide additional storage capacity, porous coccolith (Figures 3H, K, L; 19) and foraminifera test (Figure 3B–D, I) filled with OM (Figures 3F, H, I; 19H, L) can be observed in Niobrara reservoir and source rocks.

We cannot distinguish easily between solid bitumen and kerogen. But according to the criteria given by Loucks and Reed (2014), the presence of OM in fossil chambers (Figure 19L) may indicate its allochthonous character. Association of OM with anomalously large pores (Figure 19K, L) provides evidence for the emplacement of bituminized OM within a fossil body cavity. Figure 19L shows the infill of a coccolith spine by squeezed OM. The latter likely also surrounds the clay and calcite crystals at the right side and is in contact with a large pore on the upper side. The pore, having a channel-like morphology, may have acted as the pathway for moving gaseous and aqueous phases.

Assuming the fossil body cavity is indeed filled by allochthonous OM, a morphological difference might be noticeable for OM infilling intraskeletal pores (Figure 19L) and OM infilling interparticle pores (Figure 19H). Although nanopores are detected in both types, OM in intraskeletal pores seems to be less porous (i.e., denser), and OM in interparticle pores seems to have a bubble-like texture with numerous pores. It is likely that the denser OM is solid (i.e., highly viscous bitumen), which is difficult to dissolve in organic solvent (Curiale, 1986; Ko et al., 2016). In contrast, the bubble-like OM is likely the relic of less viscous bitumen after devolatilization, either naturally or artificially. Because the TEM was operated at 200 kV, devolatilization likely occurred if volatile HCs remained after FIB extraction. Considering that the maturity level of well 3 (450°C [842°F] T_{max}) is not severe enough for secondary gas generation, the bubble-like appearance of OM in well 3 (Figure 19H) can most likely be tracked back to bitumen devolatilization during sample preparation and analysis.

To avoid misunderstandings, we do not conclude that all observable OM in intraskeletal or interparticle

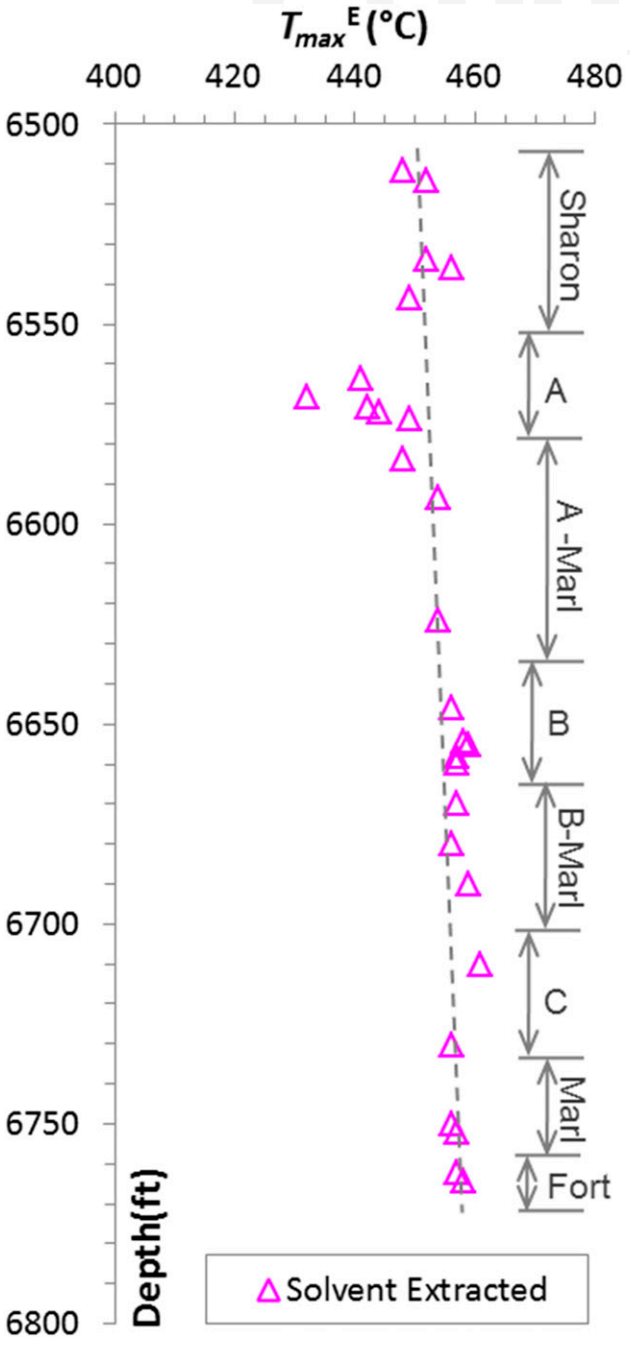

Figure 16. Geochemical depth profile of the temperature at maximum rate of petroleum generation by Rock-Eval pyrolysis detected on solvent-extracted samples (T_{max}^{E}) from well 3.

pores is solid bitumen only because nanopores are present. Nanopores can be detected more or less within all kinds of OM (bitumen as well as kerogen) in well 3 source rock and reservoir samples.

In any case, the enrichment of porous, calcareous fossils provides additional space for petroleum storage. The FIB foils extracted from reservoir rocks (Figure 19) are obviously more porous than those from source rocks (Figure 12). Interparticle pores are typically sheltered by calcite grains with straight edges (Figures 12D, K; 19), presumably coccolith skeletal debris (Figure 19B, D). Intraskeletal pores have distinct oval-equant shapes that are produced by the surrounding coccolith plates (Figure 19G, L). Abundance of both intraskeletal and interparticle pores will be enhanced as the content of carbonate fossils increases, directly resulting in the increase of producible oil in place as observed by increasing S_1 values for potential reservoir samples (carbonate >30 wt. %) (Figure 18B).

In general, and here for mudstones and marly mudstones (carbonate contents <30 wt. %), the higher the *TOC* content, the more oil is sorbed (Figure 18A). Nevertheless, oil can also be stored in the pores of calcareous fossils. Thus, for samples with carbonate contents >30 wt. % (marls to chalks), the higher the carbonate content, the more oil is stored as a fluid phase (Figure 18B), irrespective of OM richness. Therefore, because *TOC* and carbonate content are negatively correlated for the Niobrara Formation (cf. Figure 4B), the overall oil storage capacity is directly determined by carbonate content for marls to chalks (Figure 18B) and by *TOC* content for carbonate poor mudstones to marly mudstones (Figure 18A). Minimum oil-in-place values (S_1) are found for samples with approximately 20–40 wt. % carbonate content.

Regarding exploration, the best target horizons for high oil in place occur where carbonate is either low or high. Nevertheless, because sorption dominates in organic-rich mudstones, the saturation of mobile fluid-phase petroleum is likely much higher in the pore system of chalks. In addition, chalks are likely more brittle and therefore represent the primary targets in Niobrara shale oil plays.

CONCLUSIONS

The Niobrara Formation is a binary sedimentary system composed of alternating deposition of carbonate and siliciclastic minerals. As an end member of binary systems, chalk is almost purely composed of calcareous fossils (carbonate >85 wt. %). Chalks are relatively organic-poor rocks (*TOC* <2.5 wt. %) with high reservoir potential (*OSI* > 100 mg HC/g

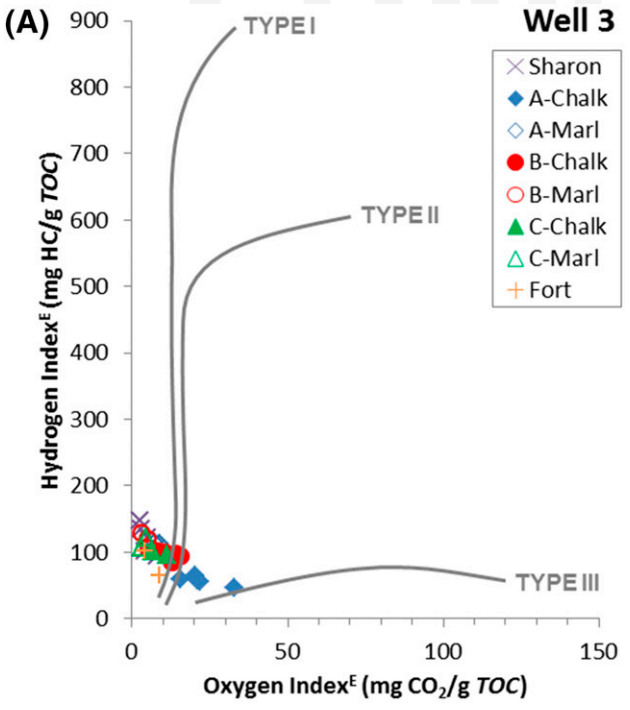

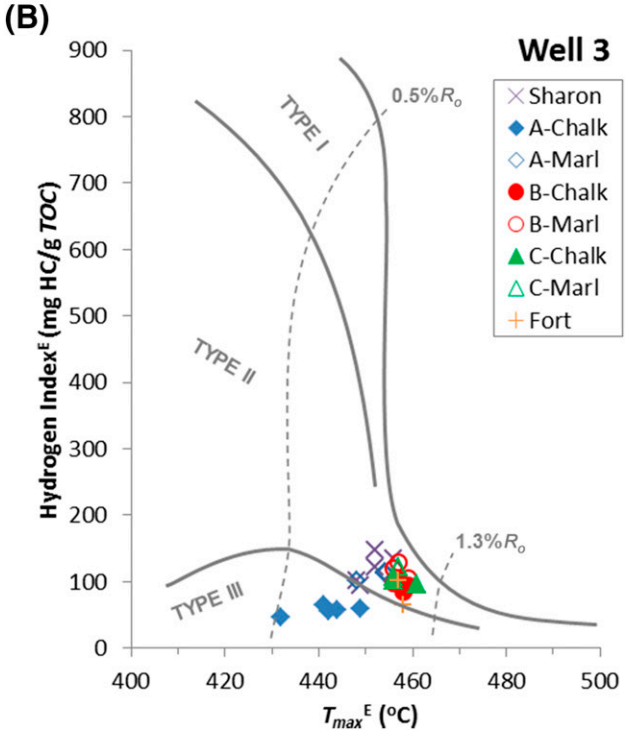

Figure 17. Crossplots of (A) hydrogen index (*HI*) versus oxygen index and (B) *HI* versus indices for the temperature at maximum rate of petroleum generation by Rock-Eval pyrolysis for solvent-extracted (E) samples. HC = hydrocarbons; R_o = vitrinite reflectance; *TOC* = total organic carbon.

TOC). As another end member, mudstone consists of mainly fine siliciclastic debris (quartz, feldspar, clay minerals, mica, etc.) with carbonate content less than 15 wt. %. Mudstones are organic-rich source rocks (*TOC* >2.5 wt. %). Marls hold intermediate positions and have carbonate contents of 70–30 wt. %. The majority of marls are treated as HC source rocks while showing partly good reservoir potential.

The majority of Niobrara source rocks can be classified as to contain type II kerogen. The most hydrogen-rich and aliphatic kerogen is present in organic-rich marl layers interbedded within the B-chalk interval, whereas types III and IV kerogen (*HI* based) is found in the A-chalk interval, Fort Hays Member, and Carlile Shale. The sample set consists of early–late oil window mature samples with T_{max} values ranging from approximately 440°C to 458°C (~824°F to 856°F). The *HI* values gradually decrease going from well 1 to well 5.

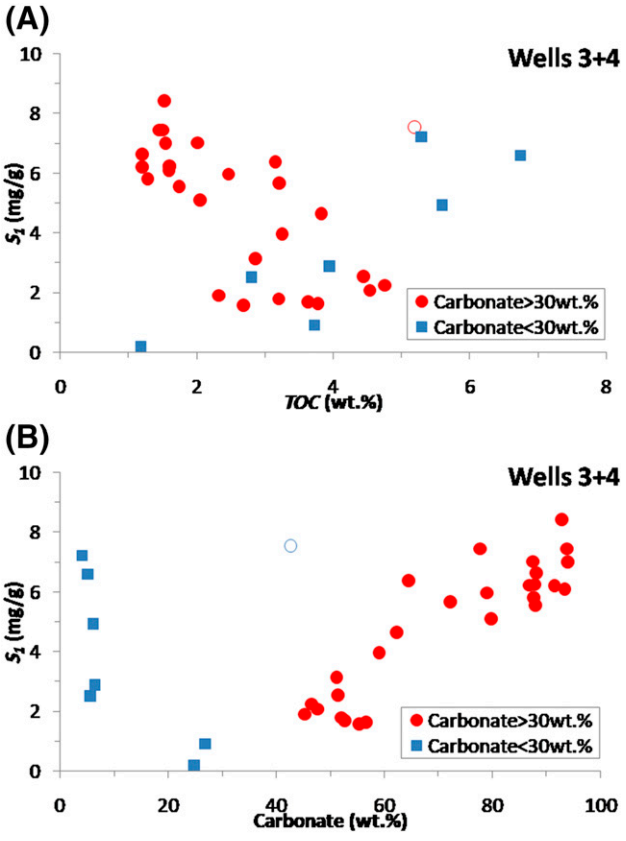

Figure 18. Crossplots of (A) S_1 versus total organic carbon (*TOC*) content and (B) S_1 versus carbonate content. The sample without fill (G015815) is an outlier.

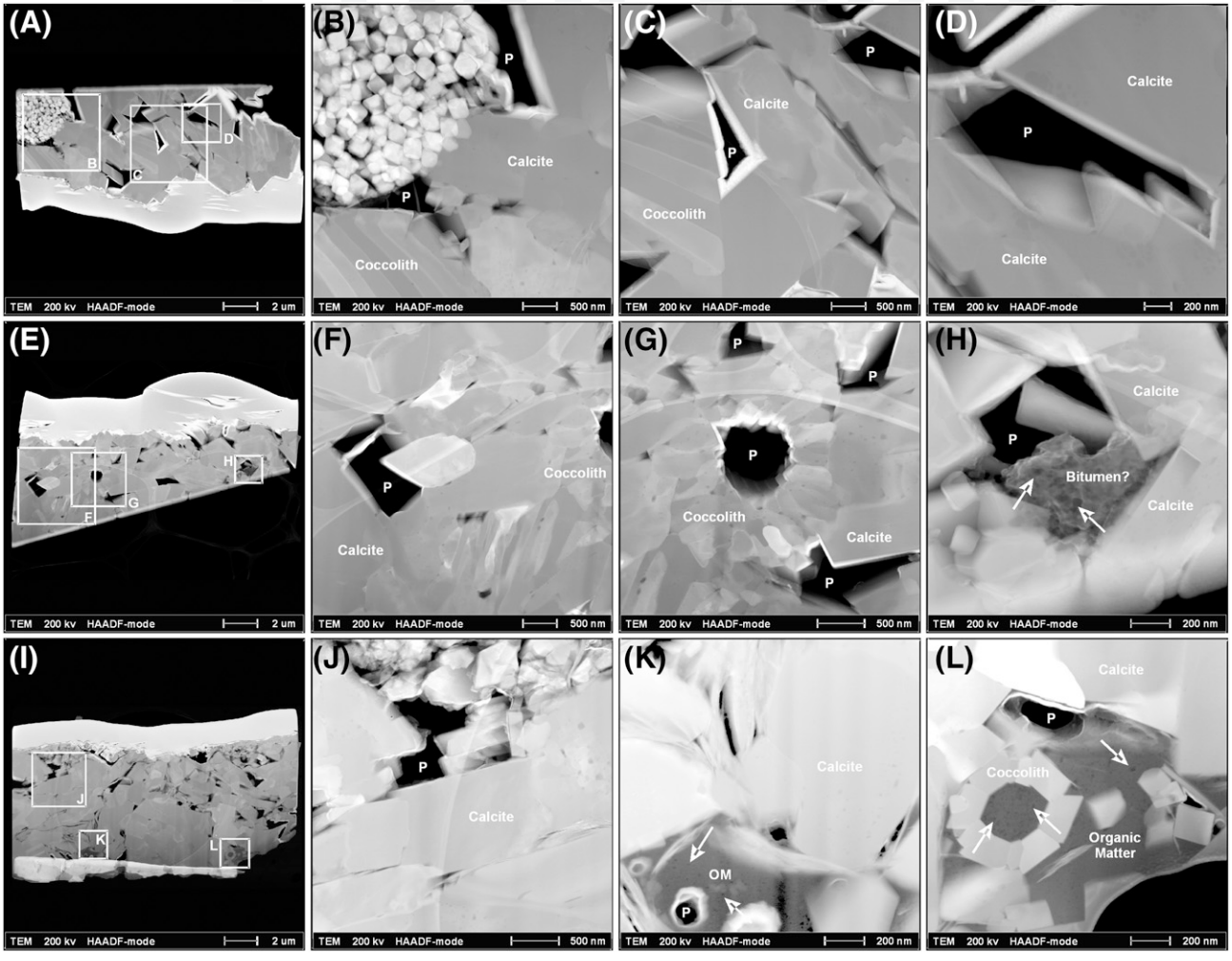

Figure 19. Transmission electron microscopy (TEM) images (high-angle annular dark-field [HAADF] mode; Z-contrast) showing mineral-associated pores (P) and organic matter associated P (white arrow). Focused ion beam foils were all extracted from chalk samples from well 3. Rectangular marked areas are magnified in following figures. (A–D) Sample G015819 from A chalk (91 wt. % carbonate; oil saturation index (*OSI)* = 512 mg of hydrocarbons (HC)/g *TOC*); mineral P associated to coccolith fragments. (E–H) Sample G015827 from B chalk (94 wt. % carbonate; *OSI* = 493 mg HC/g TOC); mineral P associated to coccolith fragments. (H) Interparticle mineral P is partly occluded by organic matter of possible bitumen origin in which bubble-like organic Ps are observed. (I–L) Sample G015834 from C chalk (88 wt. % carbonate; *OSI* = 318 mg HC/g *TOC*); mineral P and organic P are developed.

Oil retention in the source rock samples (carbonate <70 wt. %) is controlled by OM properties (i.e., OM richness and thermal maturity). In general, the higher the *T*OC, the higher the amount of retained oil (S_1). The very organic-rich marls of the B chalk are an exception and retain much less oil (per grams of *T*OC) than the other source rocks. Interestingly, kerogen in the B-chalk marls of the least mature well 1 is in contrast to that of the other source rocks in that it is highly porous. With increasing maturity, the O*SI* value of Niobrara source rock samples first increases until the maximum retention capacity (100 mg HC/g *TOC*) is exceeded at a T_{max} of approximately 445°C (~833°F) and subsequently decreases. In well 3 (T_{max} at ~450°C [~842°F]), nanopores are detected more or less in all intervals within all kinds of OM, which appears to result in a depleted oil retention capacity.

Most analyzed chalk samples (carbonate >85 wt. %) were taken from the A, B, and C chalks of well 3. Those reservoir zones are characterized by anomalously low T_{max} values. After solvent extraction, a significant shift to higher T_{max} values (>10°C [>50°F]) indicates that much of the original pyrolysis signals in fact originated from heavy petroleum compounds and not from kerogen. This is confirmed

by up to 41% of extractable *TOC*. Based on *OSI* and *HI* values, it becomes clear that more bitumen is present than could have been generated by indigenous kerogen with the A and B chalks. Thus, oil generated from the organic-rich marl layers is very likely to have migrated into those juxtaposed chalk units.

For samples with distinct reservoir potential (carbonate >30 wt. %), carbonate content is positively correlated to the amount of retained oil (S_1). Petrographic features indicate that this volatile oil is related to allochthonous OM within porous calcite fossils (i.e., coccolith and foraminifera). Although this OM infill cannot unequivocally be identified as migrated heavy petroleum, squeezed "bituminized" OM, or kerogen, it is nevertheless common sense that enrichment of porous fossils will provide additional space for the storage and flowage of petroleum fluids. Interparticle and intraskeletal OM associated with calcareous fossil fragments in chalks is more porous than that in source rocks.

Thus, overall oil retention or storage is determined by either carbonate content for samples with distinct reservoir potential (carbonate >30 wt. %) or by *TOC* content for nonreservoir rocks (carbonate <30 wt. %). Sweet spots can be expected for intervals in which carbonate content is either low or very high. However, extraction of fluid-phase petroleum from the pore space of more brittle chalk units seems to be more attractive, making chalk the primary target for the Niobrara shale oil play.

REFERENCES CITED

Baker, D. R., 1962, Organic geochemistry of Cherokee Group in southeastern Kansas and northeastern Oklahoma: AAPG Bulletin, v. 46, no. 9, p. 1621–1642.

Bergmann, J., P. Friedel, and R. Kleeberg, 1998, BGMN – A new fundamental parameters based Rietveld program for laboratory X-ray sources, it's use in quantitative analysis and structure investigations: Commission of Power Diffraction Newsletter, v. 20, no. 20, p. 5–8.

Bernard, S., B. Horsfield, H.-M. Schulz, R. Wirth, A. Schreiber, and N. Sherwood, 2012a, Geochemical evolution of organic-rich shales with increasing maturity: A STXM and TEM study of the Posidonia Shale (Lower Toarcian, northern Germany): Marine and Petroleum Geology, v. 31, no. 1, p. 70–89, doi:10.1016/j.marpetgeo.2011.05.010.

Bernard, S., R. Wirth, A. Schreiber, L. Bowen, A. Aplin, E. Mathia, H.-M. Schulz, and B. Horsfield, 2013, FIB-SEM and TEM investigations of an organic-rich shale maturation series from the Lower Toarcian Posidonia Shale, Germany: Nanoscale pore system and fluid-rock interactions, *in* W. K. Camp, E. Diaz, and B. Wawak, eds., Electron microscopy of shale hydrocarbon reservoirs: AAPG Memoir 102, p. 53–66.

Bernard, S., R. Wirth, A. Schreiber, H.-M. Schulz, and B. Horsfield, 2012b, Formation of nanoporous pyrobitumen residues during maturation of the Barnett Shale (Fort Worth Basin): International Journal of Coal Geology, v. 103, no. 0, p. 3–11, doi:10.1016/j.coal.2012.04.010.

Brian, D., W. Joel, D. Juliana, and W. S. Steven, 2013, Applications of SEM imaging to reservoir characterization in the Eagle Ford Shale, South Texas, U.S.A, *in* W. K. Camp, E. Diaz, and B. Wawak, eds., Electron microscopy of shale hydrocarbon reservoirs: AAPG Memoir 102, p. 115–136.

Claypool, G. E., and P. R. Reed, 1976, Thermal-analysis technique for source-rock evaluation: Quantitative estimate of organic richness and effects of lithologic variation: AAPG Bulletin, v. 60, no. 4, p. 608–626.

Clementz, D. M., 1979, Effect of oil and bitumen saturation on source-rock pyrolysis: AAPG Bulletin, v. 63, no. 12, p. 2227–2232.

Curiale, J. A., 1986, Origin of solid bitumens, with emphasis on biological marker results: Organic Geochemistry, v. 10, no. 1–3, p. 559–580, doi:10.1016/0146-6380(86)90054-9.

Curtis, M. E., R. J. Ambrose, C. H. Sondergeld, and C. S. Rai, 2011, Investigation of the relationship between organic porosity and thermal maturity in the Marcellus Shale: Society of Petroleum Engineers North American Unconventional Gas Conference and Exhibition, Woodlands, Texas, June 14–16, 2011, SPE-144370-MS, doi:10.2118/144370-MS.

Curtis, M. E., B. J. Cardott, C. H. Sondergeld, and C. S. Rai, 2012, Development of organic porosity in the Woodford Shale with increasing thermal maturity: International Journal of Coal Geology, v. 103, p. 26–31, doi:10.1016/j.coal.2012.08.004.

Da Gama, R. O. B. P., B. Lutz, P. Desjardins, M. Thompson, I. Prince, and I. Espejo, 2014, Integrated paleoenvironmental analysis of the Niobrara Formation: Cretaceous Western Interior Seaway, northern Colorado: Palaeogeography, Palaeoclimatology, Palaeoecology, v. 413, p. 66–80, doi:10.1016/j.palaeo.2014.05.005.

Delvaux, D., H. Martin, P. Leplat, and J. Paulet, 1990, Comparative Rock-Eval pyrolysis as an improved tool for sedimentary organic matter analysis: Organic Geochemistry, v. 16, no. 4–6, p. 1221–1229, doi:10.1016/0146-6380(90)90157-U.

Dieckmann, V., H. J. Schenk, B. Horsfield, and D. H. Welte, 1998, Kinetics of petroleum generation and cracking by programmed-temperature closed-system pyrolysis of Toarcian Shales: Fuel, v. 77, no. 1–2, p. 23–31, doi:10.1016/S0016-2361(97)00165-8.

Eglinton, T. I., J. S. Sinninghe Damsté, M. E. L. Kohnen, and J. W. de Leeuw, 1990, Rapid estimation of the organic sulphur content of kerogens, coals and asphaltenes by

pyrolysis-gas chromatography: Fuel, v. 69, no. 11, p. 1394–1404, doi:10.1016/0016-2361(90)90121-6.

Espitalié, J., 1985, Use of Tmax as a maturation index for different types of organic matter. Comparison with vitrinite reflectance, *in* J. Burrus, ed., Thermal modelling in sedimentary basins: Paris, Editions Technip, p. 475–496.

Espitalié, J., M. Madec, B. Tissot, J. J. Mennig, and P. Leplat, 1977, Source rock characterization method for petroleum exploration: Offshore Technology Conference, Houston, Texas, May 2–5, 1977, OTC-2935-MS, p. 439-444.

Espitalié, J., F. Marquis, and I. Barsony, 1984, Geochemical logging, *in* K. J. Voorhees, ed., Analytical pyrolysis: Techniques and applications: London, Butterworth-Heinemann, p. 276–304, doi:10.1016/B978-0-408-01417-5.50013-5.

Fairbanks, M. D., S. C. Ruppel, and H. Rowe, 2016, High-resolution stratigraphy and facies architecture of the Upper Cretaceous (Cenomanian–Turonian) Eagle Ford Group, Central Texas: AAPG Bulletin, v. 100, no. 3, p. 379–403, doi:10.1306/12071514187.

Frébourg, G., S. C. Ruppel, R. G. Loucks, and J. Lambert, 2016, Depositional controls on sediment body architecture in the Eagle Ford/Boquillas system: Insights from outcrops in west Texas, United States: AAPG Bulletin, v. 100, no. 4, p. 657–682, doi:10.1306/12091515101.

Han, Y., B. Horsfield, R. Wirth, N. Mahlstedt, and S. Bernard, 2017, Oil retention and porosity evolution in organic-rich shales: AAPG Bulletin, v. 101, no. 6, p. 807–827, doi:10.1306/09221616069.

Han, Y., N. Mahlstedt, and B. Horsfield, 2015, The Barnett Shale: Compositional fractionation associated with intraformational petroleum migration, retention, and expulsion: AAPG Bulletin, v. 99, no. 12, p. 2173–2202, doi:10.1306/06231514113.

Hattin, D. E., 1981, Petrology of Smoky Hill Member, Niobrara Chalk (Upper Cretaceous) in type area, Western Kansas: AAPG Bulletin, v. 65, no. 12, p. 831–849, doi:10.1306/2F919B11-16CE-11D7-8645000102C1865D.

Higley, D. K., 2015, The history of oil and gas development in the Denver Basin: AAPG Search and Discovery article 70187, accessed xx xx, xxxx, http://www.searchanddiscovery.com/documents/2015/70187higley/ndx_higley.pdf.

Higley, D. K., D. O. Cox, and R. J. Weimer, 2003, Petroleum system and production characteristics of the Muddy (J) Sandstone (Lower Cretaceous) Wattenberg continuous gas field, Denver basin, Colorado: AAPG Bulletin, v. 87, no. 1, p. 15–37.

Hill, R. J., E. Zhang, B. J. Katz, and Y. Tang, 2007, Modeling of gas generation from the Barnett Shale, Fort Worth Basin, Texas: AAPG Bulletin, v. 91, no. 4, p. 501–521, doi:10.1306/12060606063.

Horsfield, B., U. Disko, and F. Leistner, 1989, The micro-scale simulation of maturation: Outline of a new technique and its potential applications: Geologische Rundschau, v. 78, no. 1, p. 361–373, doi:10.1007/BF01988370.

Jarvie, D. M., 2012, Shale resource systems for oil and gas: Part 2—Shale-oil resource systems, *in* J. A. Breyer, ed., Shale reservoirs—Giant resources for the 21st century: AAPG Memoir 97, p. 89–119.

Jarvie, D. M., R. J. Hill, T. E. Ruble, and R. M. Pollastro, 2007, Unconventional shale-gas systems: The Mississippian Barnett Shale of north-central Texas as one model for thermogenic shale-gas assessment: AAPG Bulletin, v. 91, no. 4, p. 475–499, doi:10.1306/12190606068.

Jennings, D. S., and J. Antia, 2013, Petrographic characterization of the Eagle Ford Shale, South Texas, mineralogy, common constituents, and distribution of nanometer-scale pore types, *in* W. K. Camp, E. Diaz, and B. Wawak, eds., Electron microscopy of shale hydrocarbon reservoirs: AAPG Memoir 102, p. 101–113.

Kauffman, E. G., 1977, Geological and biological overview: Western Interior Cretaceous Basin: Mountain Geologist, v. 14, no. 3–4, p. 75–99.

Ko, L. T., R. G. Loucks, S. C. Ruppel, T. Zhang, and S. Peng, 2017, Origin and characterization of Eagle Ford pore networks in the south Texas Upper Cretaceous shelf: AAPG Bulletin, v. 101, no. 3, p. 387–418, doi:10.1306/08051616035.

Ko, L. T., R. G. Loucks, T. Zhang, S. C. Ruppel, and D. Shao, 2016, Pore and pore network evolution of Upper Cretaceous Boquillas (Eagle Ford–equivalent) mudrocks: Results from gold tube pyrolysis experiments: AAPG Bulletin, v. 100, no. 11, p. 1693–1722, doi:10.1306/04151615092.

Landon, S. M., M. W. Longman, and B. A. Luneau, 2001, Hydrocarbon source rock potential of the Upper Cretaceous Niobrara Formation, Western Interior Seaway of the Rocky Mountain region: Mountain Geologist, v. 38, no. 1, p. 1–18.

Larter, S., 1988, Some pragmatic perspectives in source rock geochemistry: Marine and Petroleum Geology, v. 5, no. 3, p. 194–204, doi:10.1016/0264-8172(88)90001-3.

Larter, S. R., 1984, Application of analytical pyrolysis techniques to kerogen characterization and fossil fuel exploration/exploitation, *in* K. Voorhees, ed., Analytical pyrolysis: Techniques and applications: London, Butterworth-Heinemann, p. 212–275, doi:10.1016/B978-0-408-01417-5.50012-3.

Lewan, M. D., and M. J. Pawlewicz, 2017, Reevaluation of thermal maturity and stages of petroleum formation of the Mississippian Barnett Shale, Fort Worth Basin, Texas: AAPG Bulletin, v. 101, no. 12, p. 1945–1970, doi:10.1306/01251716053.

Locklair, R. E., and B. B. Sageman, 2008, Cyclostratigraphy of the Upper Cretaceous Niobrara Formation, Western Interior, U.S.A.: A Coniacian–Santonian orbital timescale: Earth and Planetary Science Letters, v. 269, no. 3–4, p. 540–553, doi:10.1016/j.epsl.2008.03.021.

Loucks, R. G., and R. M. Reed, 2014, Scanning-electron-microscope petrographic evidence for distinguishing organic-matter pores associated with depositional organic matter versus migrated organic matter in mudrocks: Gulf Coast Association of Geological Societies Transactions, v. 3, p. 51–60.

Loucks, R. G., R. M. Reed, S. C. Ruppel, and D. M. Jarvie, 2009, Morphology, genesis, and distribution of nanometer-

Q:48 Q:49 Q:50

scale pores in siliceous mudstones of the Mississippian Barnett Shale: Journal of Sedimentary Research, v. 79, no. 12, p. 848–861, doi:10.2110/jsr.2009.092.

Luneau, B., M. Longman, P. Kaufman, and S. Landon, 2011, Stratigraphy and petrophysical characteristics of the Niobrara Formation in the Denver Basin, Colorado and Wyoming: AAPG Search and Discovery article 50469, accessed xx xx, xxxx, http://www.searchanddiscovery.com/documents/2011/50469luneau/ndx_luneau.pdf.

Mastalerz, M., A. Schimmelmann, A. Drobniak, and Y. Chen, 2013, Porosity of Devonian and Mississippian New Albany Shale across a maturation gradient: Insights from organic petrology, gas adsorption, and mercury intrusion: AAPG Bulletin, v. 97, no. 10, p. 1621–1643, doi:10.1306/04011312194.

Mathia, E. J., L. Bowen, K. M. Thomas, and A. C. Aplin, 2016, Evolution of porosity and pore types in organic-rich, calcareous, Lower Toarcian Posidonia Shale: Marine and Petroleum Geology, v. 75, p. 117–139, doi:10.1016/j.marpetgeo.2016.04.009.

Milliken, K. L., M. Rudnicki, D. N. Awwiller, and T. Zhang, 2013, Organic matter–hosted pore system, Marcellus Formation (Devonian), Pennsylvania: AAPG Bulletin, v. 97, no. 2, p. 177–200, doi:10.1306/07231212048.

O'Neal, D. L., 2015, Chemostratigraphic and depositional characterization of the Niobrara Formation, CEMEX Quarry, Lyons, CO, Ph.D. thesis, Colorado School of Mines, Golden, Colorado, 101 p.

Pepper, A. S., 1991, Estimating the petroleum expulsion behaviour of source rocks: A novel quantitative approach: Geological Society, London, Special Publications 1991, v. 59, no. 1, p. 9–31, doi:10.1144/GSL.SP.1991.059.01.02.

Pepper, A. S., and P. J. Corvi, 1995, Simple kinetic models of petroleum formation. Part I: Oil and gas generation from kerogen: Marine and Petroleum Geology, v. 12, no. 3, p. 291–319, doi:10.1016/0264-8172(95)98381-E.

Peters, K. E., 1986, Guidelines for evaluating petroleum source rock using programmed pyrolysis: AAPG Bulletin, v. 70, no. 3, p. 318–329, doi:10.1306/94885688-1704-11D7-8645000102C1865D.

Peters, K. E., C. C. Walters, and M. J. Moldowan, 2005, The biomarker guide: Cambridge, United Kingdom, Cambridge University Press, 1155 p.

Pollastro, R. M., 2010, Natural fractures, composition, cyclicity, and diagenesis of the Upper Cretaceous Niobrara Formation, Berthoud field, Colorado: Mountain Geologist, v. 47, no. 4, p. 135–149.

Pommer, M., and K. Milliken, 2015, Pore types and pore-size distributions across thermal maturity, Eagle Ford Formation, southern Texas: AAPG Bulletin, v. 99, no. 9, p. 1713–1744, doi:10.1306/03051514151.

Reed, R. M., and R. G. Loucks, 2015, Low-thermal-maturity (<0.7% VR) mudrock pore systems: Mississippian Barnett Shale, Southern Fort Worth Basin: Gulf Coast Association of Geological Societies, v. 4, p. 15–28.

Rice, D. D., 1984, Occurrence of indigenous biogenic gas in organic-rich, immature chalks of Late Cretaceous Age, Eastern Denver Basin, *in* J. G. Palacas, ed., Petroleum geochemistry and source rock potential of carbonate rocks: AAPG Memoir 18, p. 135–150.

Ricken, W., 1996, Bedding rhythms and cyclic sequences as documented in organic carbon-carbonate patterns, Upper Cretaceous, Western Interior, U.S: Sedimentary Geology, v. 102, no. 1–2, p. 131–154, doi:10.1016/0037-0738(95)00060-7.

Romero-Sarmiento, M.-F., M. Ducros, B. Carpentier, F. Lorant, M.-C. Cacas, S. Pegaz-Fiornet, S. Wolf, S. Rohais, and I. Moretti, 2013, Quantitative evaluation of TOC, organic porosity and gas retention distribution in a gas shale play using petroleum system modeling: Application to the Mississippian Barnett Shale: Marine and Petroleum Geology, v. 45, p. 315–330, doi:10.1016/j.marpetgeo.2013.04.003.

Sandvik, E. I., W. A. Young, and D. J. Curry, 1992, Expulsion from hydrocarbon sources: The role of organic absorption: Organic Geochemistry, v. 19, no. 1–3, p. 77–87, doi:10.1016/0146-6380(92)90028-V.

Sherwood, O. A., P. D. Travers, and M. P. Dolan, 2013, Hydrocarbon maturity and migration analysis using production gas stable isotopic signatures in the Wattenberg field, Denver Basin, Colorado, USA: Unconventional Resources Technology Conference, Denver, Colorado, August 12–14, 2013, p. 1989–1995, doi:10.1190/urtec2013-204.

Siguaw, S. G, and J. E. Estes-Jackson, 2011a, Fault Patterns in the Niobrara Formation—Examples from the Eastern and Central DJ Basin: AAPG Search and Discovery article 10354, accessed xx xx, xxxx, http://www.searchanddiscovery.com/documents/2011/10354siguaw/ndx_siguaw.pdf.

Siguaw, S. G., and J. E. Estes-Jackson, 2011b, Fault Patterns in the Niobrara Formation—Examples from the Eastern and Central Denver Basin, *in* J. E. Estes-Jackson and D. S. Anderson, eds., Revisiting and revitalizing the Niobrara in the Central Rockies: Denver, Colorado, Rocky Mountain Association of Geologists, p. 41–54.

Sonnenberg, S. A., 2011, The Niobrara petroleum system, a major tight resource play in the Rocky Mountain region: AAPG Search and Discovery article 10355, accessed xx xx, xxxx, http://www.searchanddiscovery.com/documents/2011/10355sonnenberg/ndx_sonnenberg.pdf.

Sonnenberg, S. A., and R. J. Weimer, 1993, Oil production from Niobrara Formation, Silo field, Wyoming: Fracturing associated with a possible wrench fault system: Mountain Geologist, v. 30, no. 2, p. 39–54.

Soxhlet, F., 1879, The gravimetric determination of fatty matter in milk (in German): Polytechnisches Journal, v. 232, p. 461–465.

Stainforth, J. G., and J. E. A. Reinders, 1990, Primary migration of hydrocarbons by diffusion through organic matter networks, and its effect on oil and gas generation: Organic Geochemistry, v. 16, no. 1–3, p. 61–74, doi:10.1016/0146-6380(90)90026-V.

Stock, A. T., R. Littke, J. Schwarzbauer, B. Horsfield, and C. Hartkopf-Fröder, 2017, Organic geochemistry and petrology of Posidonia Shale (Lower Toarcian, Western

Europe) – The evolution from immature oil-prone to overmature dry gas-producing kerogen: International Journal of Coal Geology, v. 176–177, p. 36–48, doi: 10.1016/j.coal.2017.04.016.

Sykes, R., and L. R. Snowdon, 2002, Guidelines for assessing the petroleum potential of coaly source rocks using Rock-Eval pyrolysis: Organic Geochemistry, v. 33, no. 12, p. 1441–1455, doi:10.1016/S0146-6380(02)00183-3.

Tanck, G. S., 1997, Distribution and origin of organic carbon in the Upper Cretaceous Niobrara Formation and Sharon Springs Member of the Pierre Shale, Western Interior, United States, Ph.D. thesis, The University of Arizona, Tucson, Arizona, 430 p.

Thul, D. J., 2012, Niobrara source rock maturity in the Denver Basin: A Study of differential heating and tectonics on petroleum prospectivity using programmed pyrolysis, Master's thesis, Colorado School of Mines, Golden, Colorado, 137 p.

Tissot, B. P., Y. Califet-Debyser, G. Deroo, and J. L. Oudin, 1971, Origin and evolution of hydrocarbons in early Toarcian shales, Paris Basin, France: AAPG Bulletin, v. 55, no. 12, p. 2177–2193.

Tissot, B. P., and D. H. Welte, 1984, Petroleum formation and occurrence: Heidelberg, Germany, Springer-Verlag, 699 p., doi:10.1007/978-3-642-87813-8.

US Energy Information Administration, 2017, Drilling productivity report for key tight oil and shale gas regions, accessed xx xx, xxxx, https://www.eia.gov/petroleum/drilling/pdf/dpr-full.pdf. Q:54

Welker, C., L. Stright, and T. Anderson, 2013, Geologic controls on oil production from the Niobrara Formation, Silo field, Laramie County, Wyoming: Unconventional Resources Technology Conference, Denver, Colorado, August 12–14, 2013, p. 146–153, doi:10.1190/URTEC2013-016.

Wirth, R., 2004, Focused ion beam (FIB): A novel technology for advanced application of micro- and nanoanalysis in geosciences and applied mineralogy: European Journal of Mineralogy, v. 16, no. 6, p. 863–876, doi:10.1127/0935-1221/2004/0016-0863.

Wirth, R., 2009, Focused ion beam (FIB) combined with SEM and TEM: Advanced analytical tools for studies of chemical composition, microstructure and crystal structure in geomaterials on a nanometre scale: Chemical Geology, v. 261, no. 3–4, p. 217–229, doi:10.1016/j.chemgeo.2008.05.019.